DYNAMICAL SYSTEMS MODELS FOR GROWTH OF RYEGRASS AND CLOVER

A THESIS PRESENTED IN PARTIAL FULFILMENT
OF THE REQUIREMENTS FOR
THE DEGREE OF MASTER OF SCIENCE IN
MATHEMATICS AT
MASSEY UNIVERSITY

Tracey Flux

February 20, 1998

Abstract

This thesis presents models formulated to describe ryegrass and clover growth independently, with the long-term goal of constructing a unified ryegrass/clover model. The purpose of this unified model will be to address the questions of co-existence of ryegrass and clover when grown together, and persistence of ryegrass in these mixed pastures.

An overview of the problem and background of the biology is provided. This may be particularly useful for the reader with no prior knowledge of ryegrass or clover biology.

A physiologically-based model for ryegrass growth is investigated. This model is a modification of that proposed by Johnson and Thornley [14] who only consider the vegetative growth phase. The modified model accounts for the reproductive growth phase. Some numerical results, with and without reproduction, are presented. These results show that increased growth occurs when reproduction is included.

A model for ryegrass growth based on tiller numbers is then investigated. This model has far fewer state variables than the above-mentioned physiologically-based model, although only vegetative growth is considered. The differential-delay equations which result from the mathematical formulation of this model are presented. Mathematical analysis of these equations reveals two steady states: a zero steady state and a finite steady state. A threshold condition that determines which of

these two steady states is eventually reached is given. The effects of harvesting the growth are also studied using numerical simulation.

Two models for clover growth, both of which are structurally similar to the second ryegrass model, are described. However the first clover model does not have any inbuilt delay mechanisms. Mathematical analysis of these models also shows the existence of two steady states: a zero steady state and a finite steady state. Again, a threshold condition determining which of these is eventually reached is given. There is little difference between the results from the two clover models, even when the numerical simulations from harvesting are considered.

Finally, a summary is given of the models studied and an indication of possible extensions to these models. A suggestion as to how a unified ryegrass/clover model might be formulated is also given.

Acknowledgements

I would like to thank Professor Robert McKibbin for his excellent guidance, and for the enthusiasm and patience he has shown during the course of this work.

I am greatly indebted to Harry Clark, Paul Newton and Ken Louie from AgResearch Limited, Grasslands for providing me with the opportunity to work on this interesting research project.

I would like to express my sincere gratitude to Ken for his considerable help during the production of this thesis, and to Harry for his much appreciated assistance with the biology.

Many thanks to my fellow graduate students for their constant enthusiasm and support, and for convincing me to learn LaTeX.

Finally, a special thank you to my family and friends for their continuous support and encouragement.

Contents

List of Figures

List of Tables

Chapter 1

Introduction

This thesis describes the investigation of dynamical mathematical models of grass and clover growth. The motivation for this work comes from a research programme at AgResearch Limited, Grasslands at Palmerston North that has a long-running interest in constructing and validating a dynamic model of population densities of grass and white clover. Of particular interest is using such a model to examine the influence management decisions have on such issues as:

- seasonal growth patterns
- persistence
- co-existence
- stability.

Dynamical systems models are particularly suitable for addressing these issues because there are well-established techniques for examining the stability of long-term solutions. Furthermore, newer techniques of bifurcation analysis (Murray [22]) can reveal the necessary conditions for "switching" between multiple long-term solutions, which is the mathematical analogue of the biological issue of persistence. Time-varying functions, which occur in describing seasonal growth, are also easily accommodated in the dynamical systems approach.

1.1 Description of the problem.

New Zealand pastoral agriculture is based on mixed grass/clover pastures, but problems arise due to the non-persistence of sown grasses (principally ryegrass) and lower than desirable proportions of white clover. The maintenance of sown grasses is deemed to be important because the benefits of new higher-yielding varieties will not be realised if they disappear from the pasture (Laidlaw and Reed [17]). A high proportion of clover is desirable because of its ability to fix nitrogen from the atmosphere and its high nutritive value (Frame and Newbold [10]).

The day to day management of pastures can influence the amount of material harvested from pastures as well as the persistence and balance of species present within a pasture community (Humphreys [12]). However, because of the large number of management options available, an experimental comparison of these options is not feasible. Constructing a model to investigate the behaviour of a two species mixture is a difficult problem and so the initial approach has been to model the behaviour of each species growing as a monoculture.

The formulated models will be described in detail in later chapters but to understand the underlying biology a brief description of the morphology and growth of grass and clover is necessary.

Grass

Grass has two morphologically different phases, vegetative and reproductive.

In the vegetative state, the grass plant consists of a collection of shoots, normally referred to as tillers (Figure 1.1), each with a short stem, known as a pseudostem (Langer [18]). The production and death of leaves is synchronised and on average each tiller comprises three fully-expanded leaves (Robson, Parsons and Williams [27]). New leaves arise from nodes at the base of the tiller. New tillers arise from

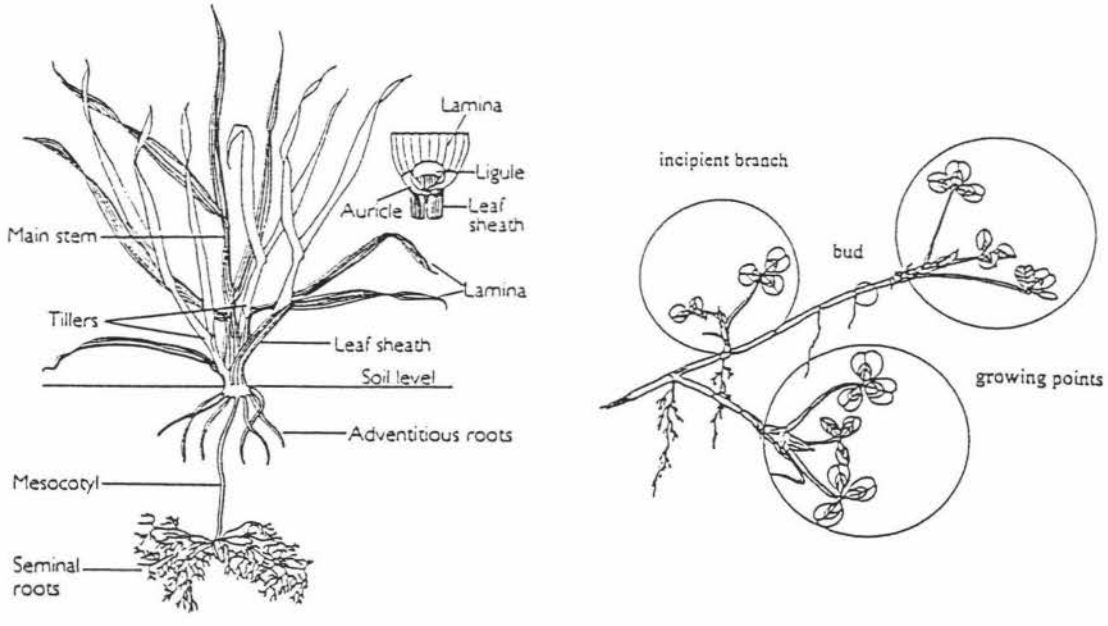

Figure 1.1: Grass plant (left) and clover plant (right)

tiller buds produced at the leaf axil. A tiller bud is produced each time a new leaf is produced. In its lifetime a ryegrass tiller produces many leaves but on average only one of the associated tiller buds develops into an adult tiller (Robson, Parsons and Williams [27]). Mature tillers (i.e. those with three fully-expanded leaves) are generally referred to as parent tillers and those with less than three leaves, daughter tillers. A vegetative ryegrass pasture therefore comprises a collection of parent tillers and their associated daughters.

The reproductive phase of grass growth is characterised by the formation of flowers and eventually seed heads on elongated stems. In the Southern Hemisphere this process begins in September/October. To change from the vegetative to the reproductive state tillers must first be vernalised, i.e. experienced winter conditions of cold temperatures and/or short day lengths (Robson, Parsons and Williams [27]). The timing of the change from the vegetative to the reproductive stage is influenced by lengthening photoperiod (daylength) and rising temperatures (Langer [18]). An

important point about reproductive tillers is that the production of a flowering stem stops the production of new leaves and the tiller therefore dies.

Clover

White clover plants are stoloniferous, consisting of a creeping network of elongated stems known as stolons (Figure 1.1). Each stolon produces nodes from its apex at regular intervals and leaves are attached by a short stem (a petiole) to each node. New stolons arise from buds (axillary buds) produced at each node. As stolons produce new nodes at the apex, older nodes die and plants fragment as they spread in a pasture (Robson, Williams and Parsons [27]). Stolons with at least three nodes are called growing points and young stolons with less than three nodes, incipient branches. The buds from which incipient branches arise can also be separated into those that are viable (those capable of producing an incipient branch under favourable conditions) and non-viable (those incapable of producing an incipient branch whatever the conditions) (Newton et al. [24]).

1.2 Survey of previous work.

Pastoral agriculture produces a large proportion of the world's milk and meat. In an effort to increase the output from pastures many models have been constructed to predict dry matter production from pastures subjected to different managements and fluctuating environmental conditions. These vary from simple regression-based models (Baars [1]) relating pasture productivity to environmental variables, through to complex dynamical systems models comprising large numbers of state variables and parameters (e.g. Johnson and Thornley [15]). Many of these models are physiologically-based where the production of new material arises from the interception of light by a leaf canopy and the production of carbon (or simply dry matter) via photosynthesis (e.g. McCall [20]; Johnson, Ameziane and Thornley [13]; Johnson and Thornley [14, 15]). These models also usually describe the

behaviour of a single species and/or a pasture where there is no attempt to differentiate between the component species (e.g. Johnson and Thornley [14, 15]; McCall [20]). Although there are some exceptions (e.g. Woodward [32]; Woodward and Wake [33]) even where these models are amenable to formal mathematical analysis this has not been attempted.

The ability of pasture plants to change the rates of tiller/growing point number production in response to both management and environmental factors is well documented (Bircham and Hodgson [4]; Jones, Collett and Brown [16]) but models looking at population dynamics in pastures based on tiller/growing point dynamics are uncommon (but see Brereton [5]; Dayan, Van Keulen and Dovrat [8]; Olsen et al. [25]). There is however a well-developed theoretical base for modelling population dynamics in both single and competing species (Begon, Harper and Townsend [2]; Begon and Mortimer [3]) and many models using plants and animals have been published. In these types of models the regulation of population numbers by processes which are density-dependent is very important (Cappaccino [7]). The main emphasis in population dynamic models is usually on survival/co-existence rather than productivity, although there are exceptions (e.g. Silliman and Gutsell [28]; Dayan, Van Keulen and Dovrat [8]; Olsen et al. [25]). Difference equations, differential equations and transition matrices have been used to construct population models (for examples see Begon and Mortimer [3]; Edelstein-Keshet [9]; Begon, Harper and Townsend [2]). In contrast to the physiologically-based models, population-based models have often been subjected to formal mathematical analysis (e.g. Guckenheimer, Oster and Ipaktchi [11]; McDonald and Watkinson [21]; Pacala [26]; Watkinson [31]).

The ryegrass (Chapter 3) and clover (Chapter 4) models constructed in this thesis attempt to combine the approaches described in the above two paragraphs. It is planned that eventually a single model will be constructed whose output will provide information on how different management strategies affect dry matter

production and the balance of species present in a ryegrass/white clover pasture. The starting point for these models is that dry matter production can be expressed simply as

(tiller/growing point) number $\times$ (tiller/growing point) size.

Therefore, the models need to incorporate population dynamics and each population unit has to have a size that changes with time. The link between the two processes is that tiller/growing point births are assumed to be dependent on the mass density of tillers/growing points. The biological justification for this density-dependent relationship is that tillers/growing points are competing for limited resources and as each unit increases in size, fewer units can be supported per unit area (Bullock [6]). A principal aim of these models is to incorporate enough biology for their behaviour to be realistic but to keep them simple enough so that they can be subjected to formal mathematical analysis.

1.3 This work.

In Chapter 2, a large, physiologically-based dynamic model for the vegetative growth of ryegrass, developed by Johnson and Thornley [14], has been extended to include reproductive growth. This model uses the idea of partitioning the above-ground dry matter into four compartments: growing leaves, first fully-expanded leaves, second fully-expanded leaves, and senescing leaves. Long-term simulations are presented, with seasonal variations in growth rate. The effects of regular harvesting are investigated. Some of the difficulties associated with this type of model are pointed out.

Chapter 3 introduces a grass growth model which treats a pasture as a population of parent tillers and daughter tillers. The use of delay in the differential equations is investigated. Numerical solutions are presented, with and without harvesting. A steady-state analysis is given along with the stability of these steady

states.

Chapter 4 investigates a model for clover which uses an approach similar to the grass model of Chapter 3 by treating clover as a population of growing points, incipient branches, and viable buds. A modification to this model introduces the use of delay in the differential equations. Steady states and their stability are investigated.

The final chapter contains conclusions drawn from working with these models. The options available for further work are also outlined.

Chapter 2

A Physiologically based Grass Model

The first of the ryegrass models to be investigated was developed by Johnson and Thornley [14]. This is a physiologically-based model of grass growth that looks in detail at the growth of the vegetative grass crop. This model was studied first, partly to provide familiarisation with MATLAB [29], but also with the aim of introducing more realistic behaviour, specifically by modifying the equations to take account of reproductive growth (refer to Section 1.1).

2.1 Model description

In the vegetative state, the grass plant consists of a collection of shoots, or tillers (Figure 2.1). As described in Section 1.1, there are three live fully-expanded leaves per tiller. This vegetative crop growth model divides the total above-ground structural crop into four compartments corresponding to growing leaves, first fully-expanded leaves, second fully-expanded leaves, and senescing leaves. This model is based on the flow of carbon between these leaves [kg (carbon) m^{-2} (ground)], and the leaf area development of each leaf [m^2 (leaf) m^{-2} (ground)]. The nine state variables are: leaf area indices for each compartment, L_1, L_2, L_3, L_4; structural weights of each compartment, W_1, W_2, W_3, W_4; and a single storage component,

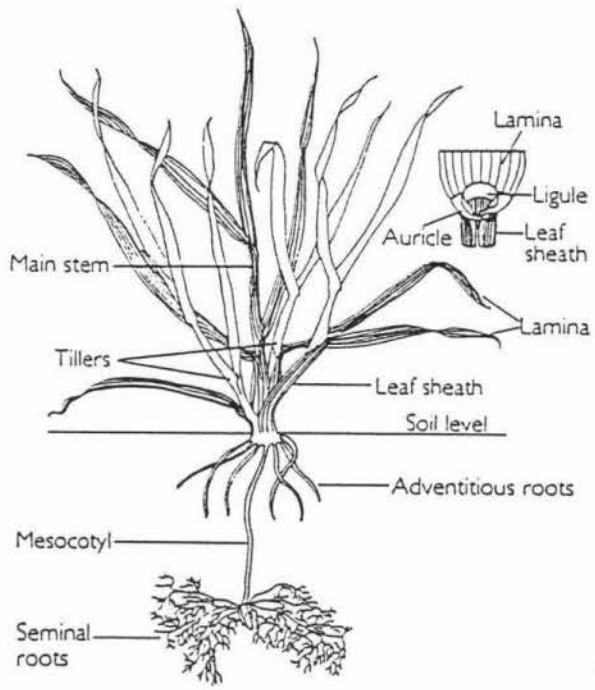

Figure 2.1: A grass plant

W_S. The total structural weight W_G is

$$W_G = \sum_{i=1}^{4} W_i$$

and the total crop weight is

$$W = W_G + W_S.$$

The total leaf area index (LAI) is given by

$$L = \sum_{i=1}^{4} L_i.$$

The storage compartment, W_S, is supplied with carbon by photosynthesis which is utilised for new structural growth and maintenance. Photosynthesis is related to light intensity and the precise relationship is shown in light-response curves (Thornley [30]). One curve (Johnson and Thornley [15]) used to describe the relationship between the photosynthetic rate, P_g, and the light flux intensity,

I_l, is a non-rectangular hyperbola with equation

$$\theta P_g^2 - (\alpha I_l + P_m)P_g + \alpha I_l P_m = 0 \tag{2.1}$$

where

I_l	is the light flux density on the leaf	[J m^{-2} (leaf) s^{-1}]
θ	is a dimensionless parameter	$(0 \leq \theta \leq 1)$
α	is the photosynthetic efficiency	[kg (CO_2) J^{-1}]
P_m	is the asymptotic value of P_g at high light	[kg (CO_2) m^{-2} (leaf) s^{-1}].

The single leaf photosynthetic rate, P_g [kg (CO_2) m^{-2} (leaf) s^{-1}], is given by the smaller root of Equation (2.1),

$$P_g = \frac{1}{2\theta}\left[(\alpha I_l + P_m) - \sqrt{(\alpha I_l + P_m)^2 - 4\theta\alpha I_l P_m}\right].$$

The canopy gross photosynthetic rate, P_c, is obtained by integrating P_g over the leaf area index L,

$$P_c = \int_0^L P_g(I_l)\, dl.$$

To evaluate this integral it is assumed that the light flux density incident on the surface of a leaf at depth L, is related to the instantaneous light flux density above the canopy, I_0, by

$$I_l = \left(\frac{k}{1-\tau}\right) I_0\, e^{-kl}$$

where k is the canopy extinction coefficient and τ is the leaf transmittance.

The following integral gives the daily carbon input P [kg (carbon) m^{-2}] day^{-1}

$$P = \phi\,\Theta \int_0^h P_c\, dt$$

where h is the daylength [seconds], Θ is a factor to convert CO_2 to carbon and ϕ is the fraction available for shoot growth.

The rate of synthesis of new structural material, G [kg m^{-2} day^{-1}] is given by

$$G = \mu \frac{W_S W_G}{W}$$

where μ is a rate constant.

A yield factor Y is defined as the proportion of carbon in the substrate carbon pool used to produce a new structure. Thus the rate of utilisation of the substrate carbon for new growth is G/Y.

Maintenance respiration is assumed to be proportional to the plant dry weight, and varies between the different compartments W_i, i =1–4. The total maintenance respiration is given by

$$R_m = \sum_{i=1}^{4} M_i W_i$$

where the M_i, i = 1–4 are maintenance coefficients.

It is assumed that the flux of material from W_1 to W_2, W_2 to W_3, and W_3 to W_4 depend on the leaf appearance rate, γ. The weight of the average leaf passing from W_1 to W_2 will be considerably greater than the average leaf weight in W_1 as this compartment comprises growing leaves. Therefore, the flux of live structure from W_1 to W_2 is given by

$$\lambda \gamma W_1$$

where the weighting factor λ allows for the difference in leaf weight.

Senescence, described by the flux of material out of W_4, is also dependent on the rate of leaf appearance γ.

The rate of production of new leaf area is

$$\delta \rho G$$

where ρ is the fraction of new growth which is partitioned to leaf growth and δ is treated as the incremental specific leaf area. It is assumed that

$$\delta = \delta_m \left(1 - \zeta \frac{W_S}{W}\right)$$

where δ_m is the maximum value of the leaf area to leaf weight ratio, and ζ is an incremental specific leaf area parameter.

The flow of material from L_1 to L_2, L_2 to L_3, and L_3 to L_4 depend on the leaf appearance rate, γ. Also, the flux of material from L_1 to L_2 is weighted by the factor λ, and is given by

$$\lambda \gamma L_1.$$

The differential equations, describing the flow of carbon between compartments, are:

$$\frac{dW_s}{dt} = P - G/Y - R_m \tag{2.2}$$

$$\frac{dW_1}{dt} = G - \lambda \gamma W_1 \tag{2.3}$$

$$\frac{dW_2}{dt} = \lambda \gamma W_1 - \gamma W_2 \tag{2.4}$$

$$\frac{dW_3}{dt} = \gamma W_2 - \gamma W_3 \tag{2.5}$$

$$\frac{dW_4}{dt} = \gamma W_3 - \gamma W_4 \tag{2.6}$$

$$\frac{dL_1}{dt} = \delta \rho G - \lambda \gamma L_1 \tag{2.7}$$

$$\frac{dL_2}{dt} = \lambda \gamma L_1 - \gamma L_2 \tag{2.8}$$

$$\frac{dL_3}{dt} = \gamma L_2 - \gamma L_3 \tag{2.9}$$

$$\frac{dL_4}{dt} = \gamma L_3 - \gamma L_4 \tag{2.10}$$

where the derived variables and units[1] are defined in Table 2.1, and parameters with their estimates in Table 2.2. Derived variables can be obtained once the values of the state variables are known. For example, $G = \mu \frac{W_S W_G}{W}$ can be calculated from knowledge of W_i, $i = 1$–4, and W_S.

Seasonal variations

The parameters which vary with season are

T	mean daily temperature	°C
h	daylength	seconds
J	daily energy (photosynthetically active radiation, PAR)	J m^{-2}.

The rate parameter γ, growth coefficient μ, maintenance coefficients M_i, and light-saturated gross photosynthetic rate P_m, increase linearly as temperature increases by the factor

$$\frac{T - T_0}{20 - T_0},$$

where T_0 (taken to be 0°C) is the temperature where crop growth effectively ceases.

The instantaneous light flux density above the canopy, which is required to calculate the total daily photosynthetic input available for shoot growth, is directly proportional to the daily energy

$$I_0 = J/h.$$

The environmental parameters T, h and J were read from a weather datafile in the simulations of Section 2.3. That is, values for T, h and J were known throughout the period when the simulations were carried out.

[1] Unless otherwise stated, mass (kg) refers to carbon and area (m^2) refers to ground.

Derived Variable	*Biological meaning*	*Units*
G	Rate of production of new structure	kg m^{-2} day^{-1}
I_l	Instantaneous light flux density on the leaves at leaf area index L	J m^{-2} s^{-1}
L	Leaf area index of crop	m^2 (leaf) m^{-2}
P	Total daily carbon input to the shoot	kg m^{-2} day^{-1}
R_m	Maintenance respiration	kg m^{-2} day^{-1}
W	Total crop dry weight	kg m^{-2}
W_G	Total structural dry weight	kg m^{-2}
δ	Incremental specific leaf area	m^2 (leaf) kg^{-1}

Table 2.1: Derived variable definitions for Johnson/Thornley model

Parameter	*Biological meaning*	*Estimated value*
k	Extinction coefficient of canopy	0.5
M_i $i = 1$–4	Maintenance respiration coefficients	day^{-1} depends on temperature
P_m	Light-saturated gross photosynthetic rate - vegetative value, reproductive value	kg (CO_2) m^{-2} s^{-1} depends on temperature
Y	Yield factor	0.75
α	Leaf photosynthetic efficiency - vegetative value - reproductive value	 10×10^{-9} kg (CO_2) J^{-1} 12×10^{-9} kg (CO_2) J^{-1}
γ	Rate of leaf appearance	day^{-1} depends on temperature
δ_m	Maximum value of leaf area/leaf weight ratio	40 m^2 (leaf) kg^{-1}
ζ	Incremental specific leaf area parameter	1
θ	Leaf photosynthesis parameter	0.95
Θ	Conversion factor from CO_2 to carbon	12/44
λ	Weighting factor for flux of material from first component to second component	2
μ	Growth coefficient	depends on temperature
ρ	Fraction of new growth partitioned to leaf growth	0.7
τ	Leaf transmission coefficient	0.1
ϕ	Proportion of carbon fixed partitioned above ground	0.9

Table 2.2: Parameter definitions for Johnson/Thornley model

Modifications for Reproductive Growth

As explained in Section 1.1, the rate of reproductive growth is higher than the rate of vegetative growth. To model this behaviour, the photosynthetic efficiency, α, and asymptotic value of P_g at high light, P_m, (Equation 2.1) have been modified as follows.

Grass growth is assumed to be vegetative until August 1st when reproductive growth commences. Both α and P_m are increased linearly to reach the higher reproductive α and P_m values when daylength, h, is 10.5 hours (37800 seconds). These reproductive values continue until the accumulated daily average temperatures reach 500°C, when α and P_m are decreased in a linear manner, to again be at the vegetative values on December 31. Using the weather datafile, the days obtained were 32, 77, 167, and 184, corresponding to August 1, September 15, November 14, and December 31 respectively. Figure 2.2 shows the change in values for P_m.

Figures 2.3, 2.4, 2.5, 2.7 and 2.8 show vegetative grass growth (dotted lines) and the addition of reproductive growth (solid line).

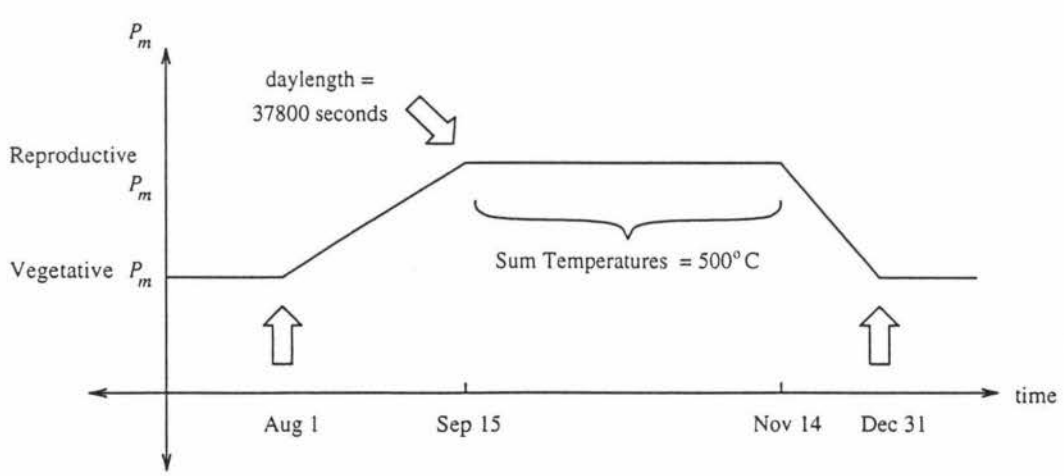

Figure 2.2: Varying P_m over time

2.2 Calculations (simulations)

2.2.1 Method of calculation.

The set of simultaneous ordinary differential equations (ODEs), (2.2)–(2.10), were solved numerically using a fourth and fifth order Runge-Kutta ODE solver in MATLAB [29]. A time step of one day was used. Decreasing the time step had no significant effect on the solutions. The differential equations were integrated over one year (365 days), where day one represents July 1. Reproductive growth begins at day 32 and finishes on day 184.

2.2.2 Initial conditions.

The initial conditions for W_S and the W_i and L_i, i = 1–4, were chosen to be arbitrary small values, as follows:

$$W_S(0) = 0.005 \text{ g m}^{-2} \qquad L_1(0) = 0.2$$
$$W_1(0) = 0.010 \text{ g m}^{-2} \qquad L_2(0) = 0.2$$
$$W_2(0) = 0.010 \text{ g m}^{-2} \qquad L_3(0) = 0.2$$
$$W_3(0) = 0.010 \text{ g m}^{-2} \qquad L_4(0) = 0.2$$
$$W_4(0) = 0.010 \text{ g m}^{-2}.$$

2.3 Results of calculations

The results of running this model with initial conditions as given in Section 2.2.2, for one year, are shown in Figure 2.3.

These solution curves show that constant values are approached at large time. The dotted lines show the solutions obtained before modifications for reproductive grass growth were added. For all components the effect of reproductive growth is to enhance the structural dry weight or leaf area index during the reproductive

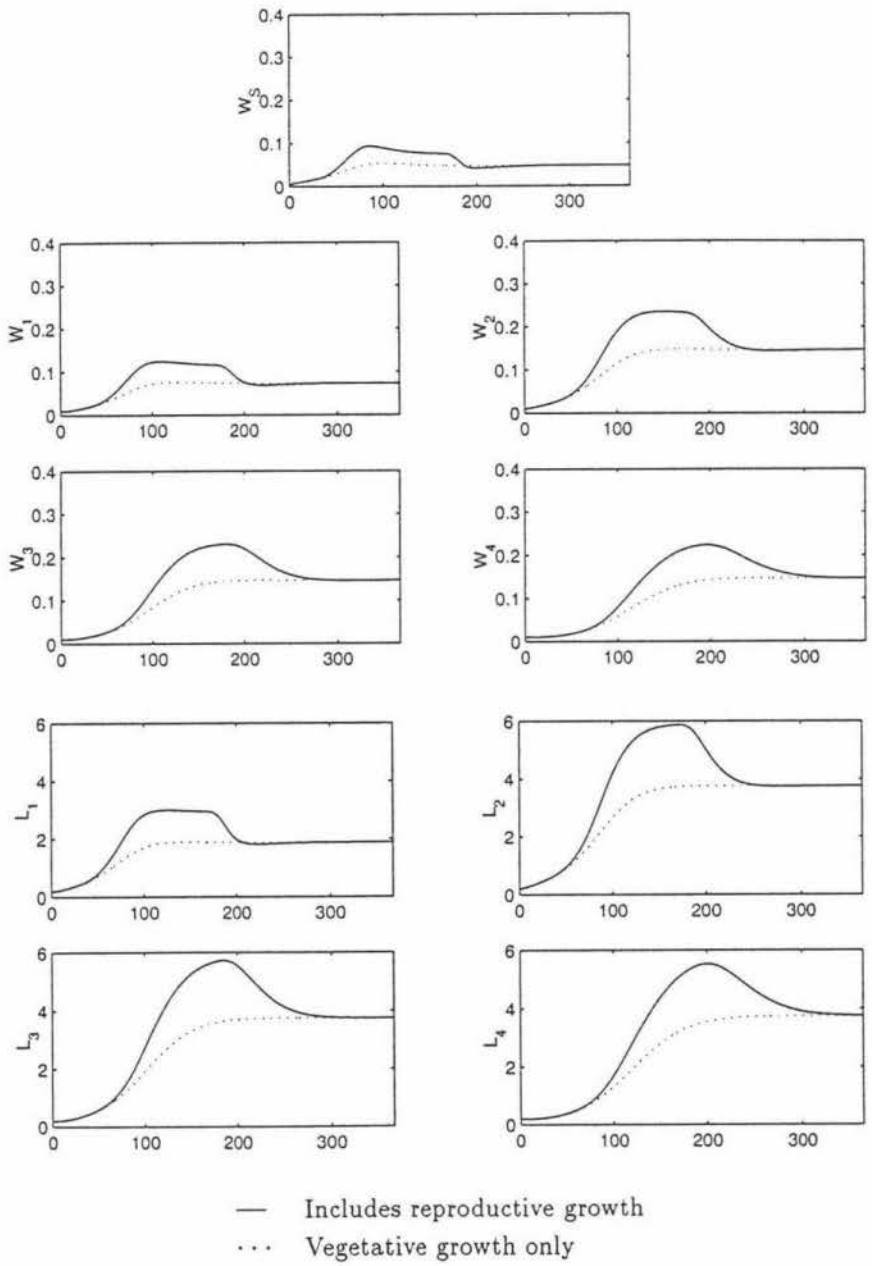

Figure 2.3: Plots of the structural dry mass components and leaf area indices vs time with initial conditions as given in Section 2.2.2

period, as expected biologically. The effect is more pronounced in the third and fourth leaf components (W_3, W_4, L_3 and L_4) where the solution curves do not coincide until well past day 250, although the reproductive period ends on day 184.

Figure 2.4 compares the structural storage weight, W_S, with the sum of the structural weight in the four leaf compartments, W_G. Most of the structural weight is in the leaves. The total structural weight ($W_S + W_G$), and leaf area index are also shown. They both reach maximum values at approximately 180 days, corresponding to the time when most of the grass crop is growing reproductively. After approximately 250 days, the total structural weight "settles" at around 0.6 kg m^{-2}, and the leaf area index around 13.

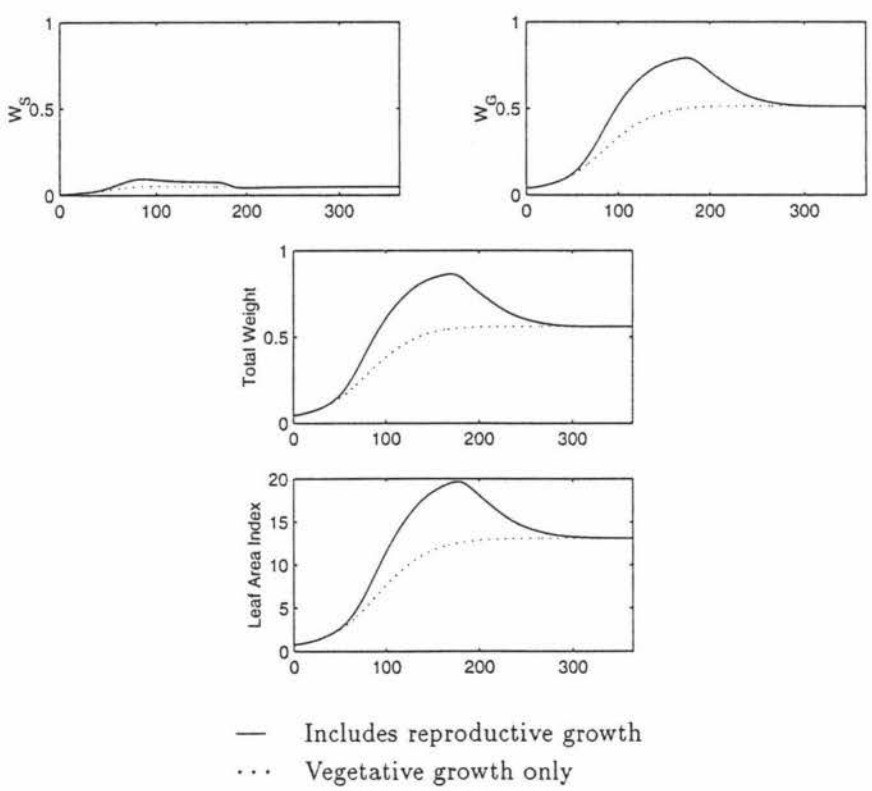

Figure 2.4: Plots of total structural weight and leaf area index vs time

Trajectories of solutions to Equations (2.2)–(2.10) are curves in nine-dimensional space. These cannot be displayed, so Figure 2.5 shows projections of these curves on to some appropriate plane. For example, the first plot is a projection on to the W_1–W_S plane. The '+' indicate time intervals of 30 days, where the starting time t_0 is shown by 'o'. These plots show that steady values for all structural weight components are being approached as t increases because the size of the intervals between the '+' is becoming very small. The dotted lines in Figure 2.5 are projections of the solution curves which only consider vegetative growth. They also converge to the same steady values as the solution curves with reproductive growth which have been seen in Figures 2.3 and 2.4.

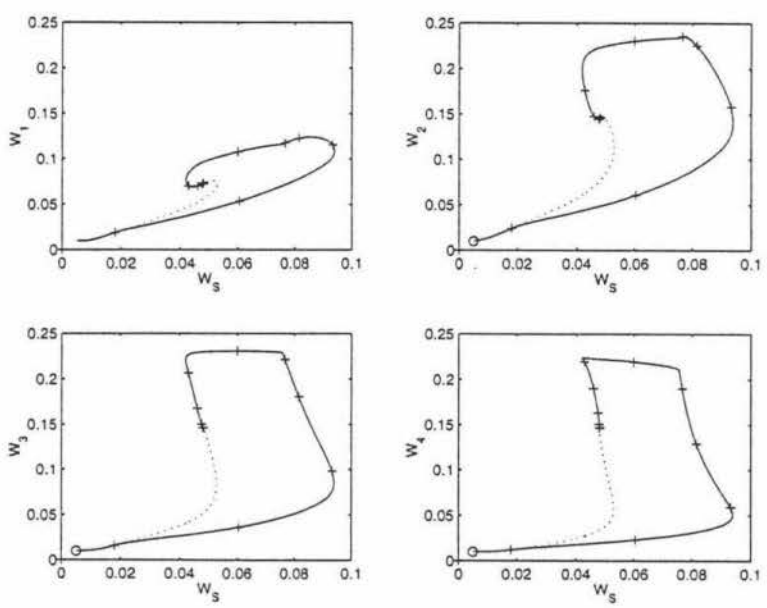

Figure 2.5: Projection of trajectories onto W_i–W_S, i=1–4, planes

Sensitivity to Initial Conditions

Only the model modified to exhibit reproductive growth is used to investigate the sensitivity to the initial conditions. Figure 2.6 shows the total structural weight and leaf area index vs time, with four different initial conditions. The solid line shows the curves with initial conditions as given in Section 2.2.2. The dotted curve has initial conditions for the total structural weight multiplied by ten and the leaf area indices unchanged, the dashed line has initial conditions for the total structural weight unchanged and the leaf area indices multiplied by ten, and in the last curve initial conditions for both structural weight and leaf area indices are multiplied by ten.

It is found that this model is not sensitive to the initial conditions and all curves follow the same path after about 200 days.

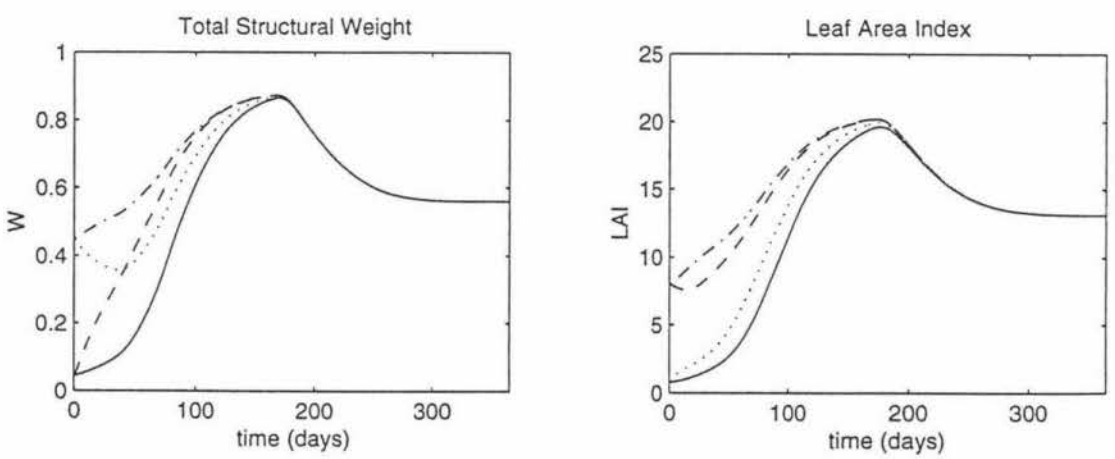

	[W_S	W_1	W_2	W_3	W_4	L_1	L_2	L_3	L_4]
—	[0.005	0.01	0.01	0.01	0.01	0.2	0.2	0.2	0.2]
···	[0.050	0.10	0.10	0.10	0.10	0.2	0.2	0.2	0.2]
– –	[0.005	0.01	0.01	0.01	0.01	2.0	2.0	2.0	2.0]
·–·	[0.050	0.10	0.10	0.10	0.10	2.0	2.0	2.0	2.0]

Figure 2.6: Total structural weight and leaf area index with different initial conditions as stated above

2.4 Harvesting

At harvest the total structural weight, W, is reduced to the original total weight. The leaf area indices are then reduced by the same proportion.

To describe this quantitatively, let H be days between harvests, a superscript '-' indicates time immediately prior to the harvest and a superscript '+' indicates time immediately after a harvest, i.e.

nH^- is the time immediately prior to the nth harvest,

nH^+ is the time immediately after the nth harvest.

Define the proportion by which the weight and leaf components are reduced at harvest n by

$$c_n = \frac{W_S(0) + \sum_{i=1}^{4} W_i(0)}{W_S(nH^-) + \sum_{i=1}^{4} W_i(nH^-)}. \tag{2.11}$$

The values of the weight and leaf components immediately after harvest n are

$$\begin{aligned} W_S(nH^+) &= c_n W_S(nH^-) \\ W_i(nH^+) &= c_n W_i(nH^-) \\ L_i(nH^+) &= c_n L_i(nH^-) \end{aligned}$$

for $i = 1$–4, $n = 1, 2, 3, \ldots$

The results obtained by simulating harvesting are shown in Figure 2.7. The reproductive and vegetative phases of grass growth are represented by the solid lines and dotted lines respectively. They differ during the reproductive phase but coincide after approximately 200 days. The solution curves appear to have reached a repeating pattern corresponding to c_n tending to some constant value as n increases.

The total weight, W, and the total Leaf Area Index, L, against time in Figure 2.8 shows the enhanced growth rate over the reproductive phase. This figure also shows the cyclic behaviour exhibited in Figure 2.7.

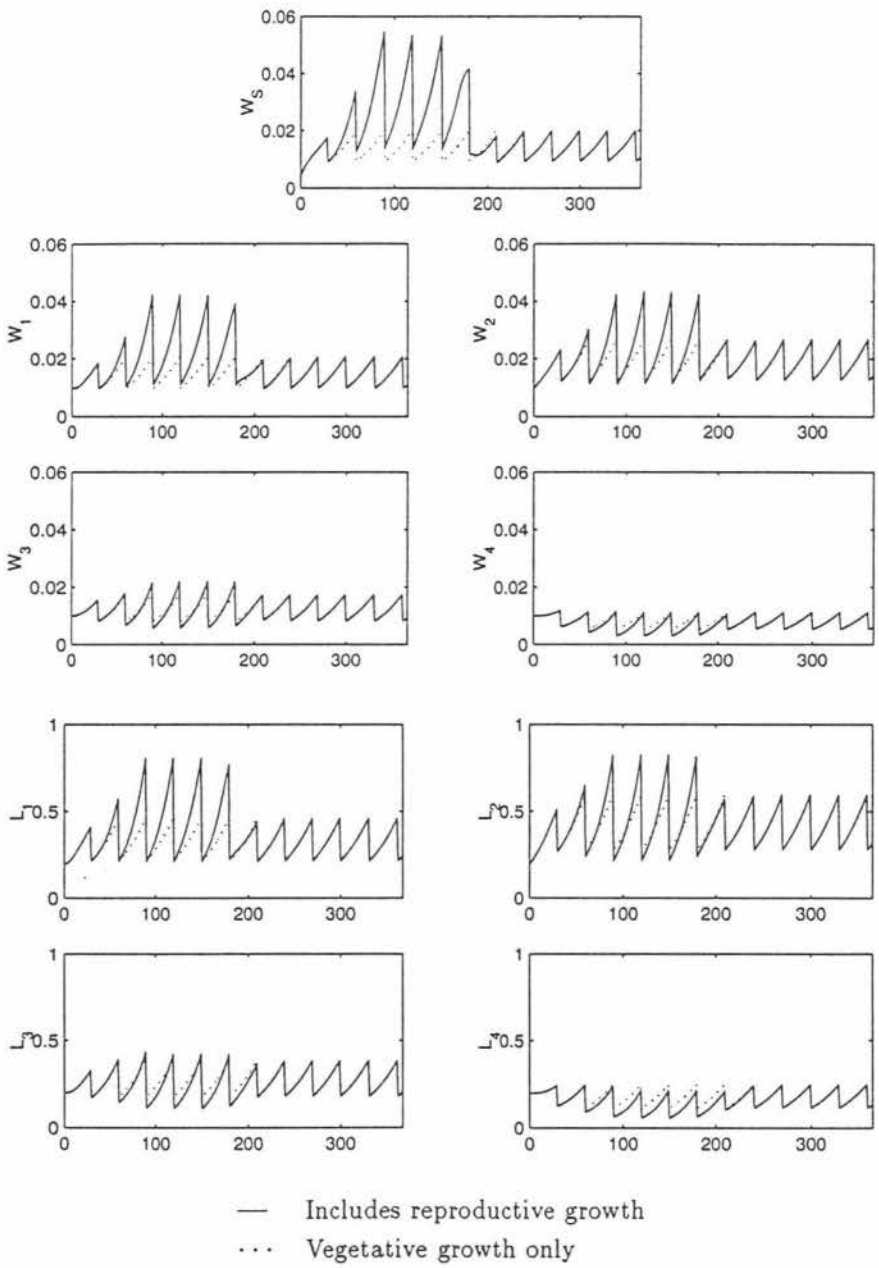

Figure 2.7: Plots of the structural dry mass components and leaf area indices vs time with initial conditions as given in Section 2.2.2 and a harvesting interval of 30 days

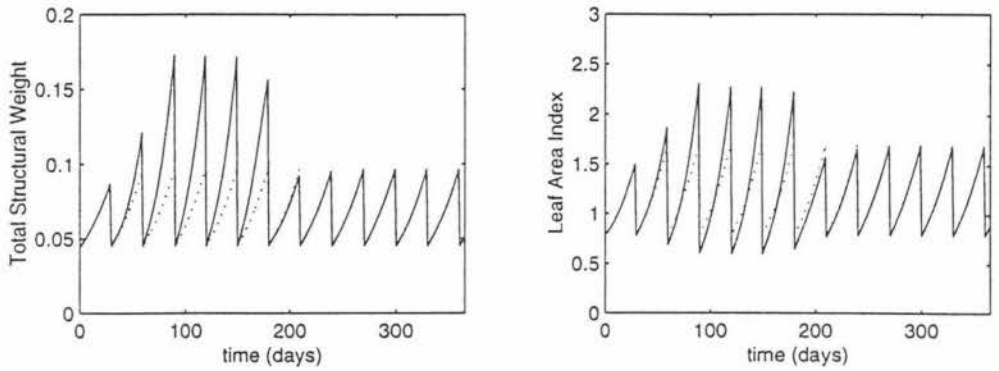

— Includes reproductive growth
· · · Vegetative growth only

Figure 2.8: Plots of total structural weight and leaf area index with harvesting every 30 days

The trajectories are curves in nine-dimensional space. Figure 2.9 illustrates projections of the solution curves on to two-dimensional planes, namely the W_S–W_i, $i = 1$–4 planes. The starting time, t_0, is indicated by 'o' in Figure 2.9. Since the harvesting interval is 30 days, each 'segment' represents 30 days.

The cyclic behaviour seen in Figures 2.7 and 2.8 is shown in Figure 2.9 by the 'segments' following repeating paths. There appears to be two separate cyclic paths, especially noticable in the third plot of Figure 2.9 (W_3 against W_S). These reflect the two different growth rates resulting from vegetative and reproductive grass growth.

Similar graphs were obtained from plotting the other state variables in this nine-dimensional model.

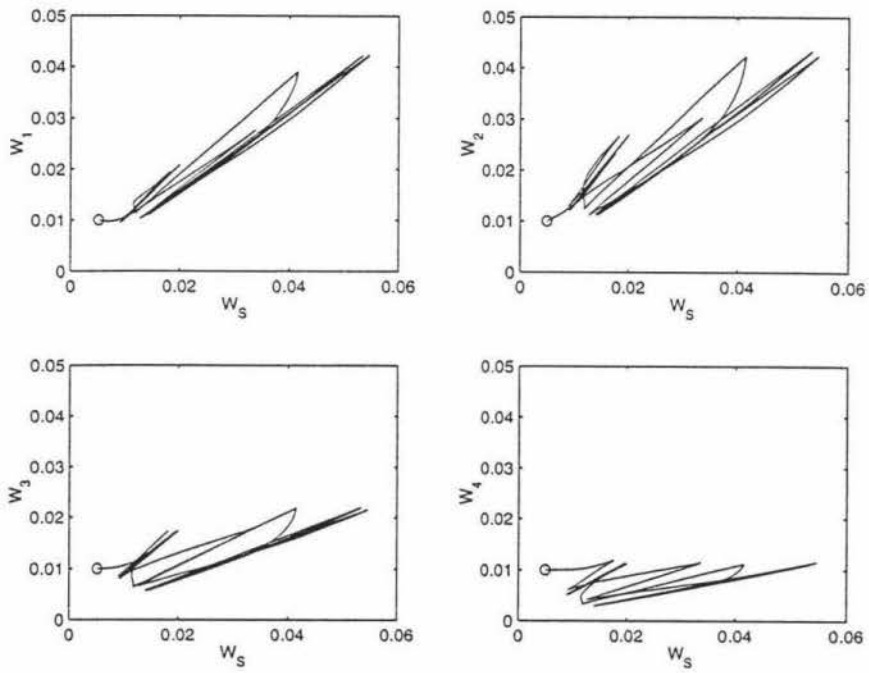

Figure 2.9: Projection of trajectories with harvesting

Sensitivity to Initial Conditions

The sensitivity to the initial conditions was investigated for the model with reproductive growth incorporated. The initial values of each weight component was doubled while the initial values for the leaf area indices remained as in Section 2.2.2. Figure 2.10 shows that it does not return to the same cycle as the original initial conditions. However, changing the initial conditions for the leaf area indices to ten times the original showed no effect on the long-term behaviour of the model (Figure 2.11).

The solution curves do not return to the same cycle when the initial values for the weights are changed because the procedure used for harvesting (Section 2.4) is dependent on the initial total structural weight.

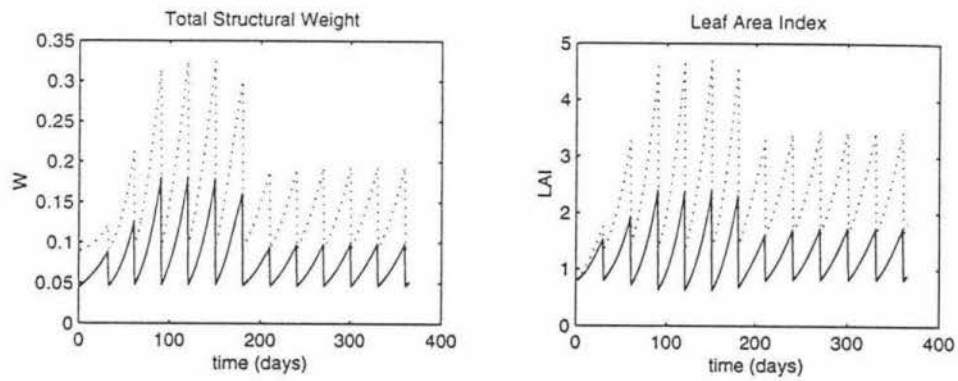

— initial conditions as given in Section 2.2.2
... intitial conditions for Total Structural Weight (×2)

Figure 2.10: Total structural weight and leaf area index with changed initial conditions for weight

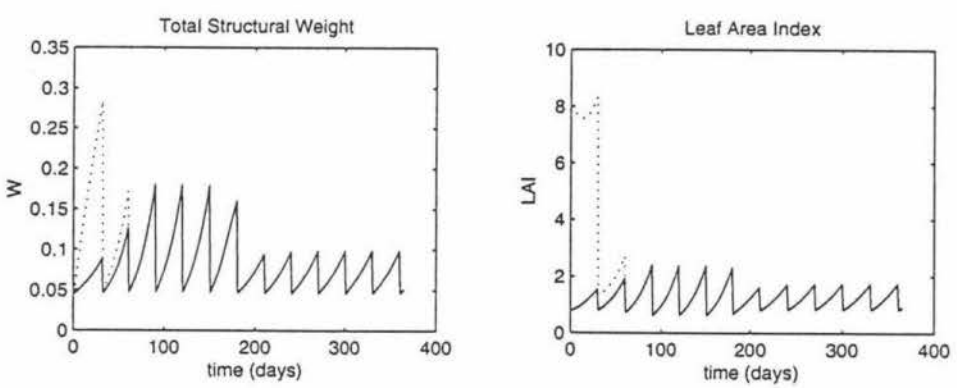

— initial conditions as given in Section 2.2.2
... intitial conditions for Leaf Area Indices (×10)

Figure 2.11: Total structural weight and leaf area index with changed initial conditions for leaf area indices

2.5 Summary and Comments

Numerical solutions were obtained for this model for both vegetative growth and reproductive growth of ryegrass. These simulations showed that steady states were being reached. However, because of the complexity of the model, it is difficult to obtain this steady state analytically.

Another drawback in this model is the large numbers of parameters. There remains the problem of estimating their values biologically, rather than merely providing some plausible values (as in Tables 2.1 and 2.2).

For these reasons, attention is directed to smaller models in the following two chapters. These models are not physiologically (carbon) based but take as their fundamental unit the tiller for ryegrass or the growing point for clover.

Chapter 3

A Tiller based Grass Model

The next model to be investigated describes the growth of a typical grass (e.g. ryegrass) in terms of tillers. This model considers only vegetative grass growth.

3.1 Model Description

A grass plant consists of a collection of tillers. Tillers are classified as either daughter tillers or parent tillers (see Figure 3.1). Each parent tiller has three live leaves. Daughter tillers have less than three leaves, and arise from buds in axils of leaves.

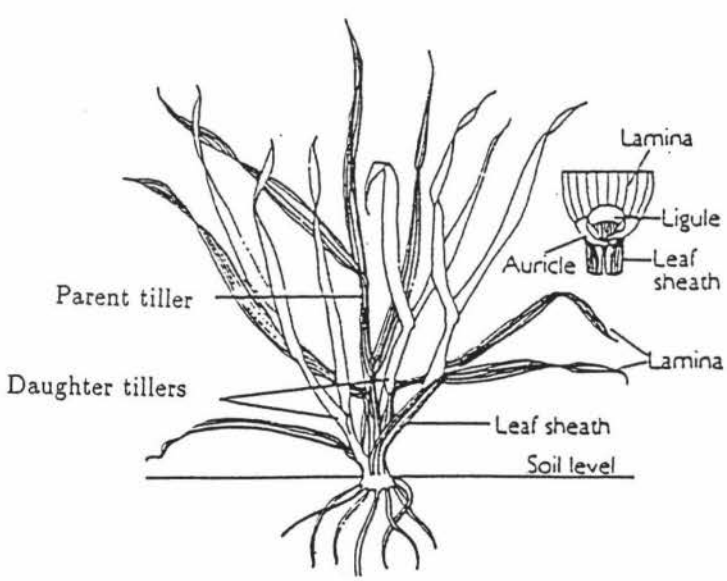

Figure 3.1: Grass plant with tillers

The model is based on the representation of ryegrass tillers as comprising two interacting state variables, the number densities of Parent tillers (P), and Daughter tillers (T), see Figure 3.2.

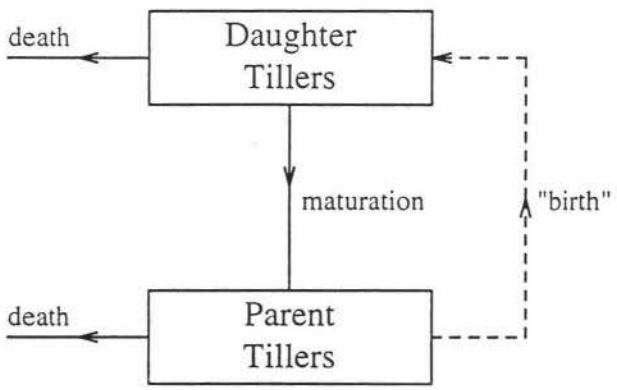

Figure 3.2: Conceptual diagram of tiller-based grass model

From Figure 3.2, the processes governing the change in daughter tiller numbers are: two outward flows depleting the daughter tiller pool, namely maturation of daughter tillers into parent tillers and death of daughter tillers; and one inward flow, the "birth" of daughter tillers.

The birth rate of daughter tillers is dependent on the mass density of parent tillers. This mass density is defined as the product of parent tiller number density P (m^{-2}) and the average parent tiller size S (g) at that time. The density dependence is introduced to model the effect of "crowding" and means that the likelihood of a parent tiller giving rise to a daughter tiller is lower when the mass density of parents is high, as shown in Figure 3.3. The mathematical formulation for this is given by:

$$\frac{A^2\ L\ P(t)}{C^2 + [S(t)\ P(t)]^2}$$

where L is the leaf appearance rate and $(\frac{A}{C})^2$ is the likelihood of a parent tiller giving rise to a daughter when the parent mass density is zero.

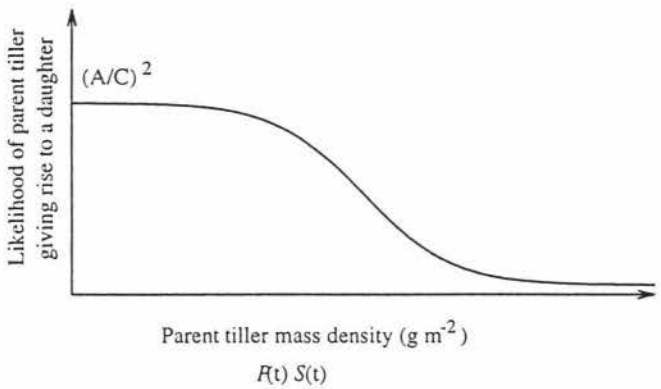

Figure 3.3: Likelihood of parent tiller giving rise to a daughter vs parent tiller mass density

The death of daughter tillers is purely random and the result of some accidental outside influence. Mathematically, the death rate of daughter tillers is given by

$$\beta\, D(t).$$

Since a tiller is classified as a daughter tiller until it has three leaves, the maturation interval is two leaf appearance intervals. Therefore, the daughters which become parents at time t depends on the number of daughter tillers "born" two leaf appearance intervals earlier, $(t - \frac{2}{L})$, scaled by a factor, $\exp(\frac{-2\beta}{L})$, which takes into account the "random" deaths of these daughter tillers over this time interval. This neccessitates the introduction of a delay term into this model. Mathematically, the rate of maturation of daughters into parent tillers is given by

$$\frac{A^2 L\, P(t - \frac{2}{L})\, \exp(\frac{-2\beta}{L})}{C^2 + [S(t - \frac{2}{L})\, P(t - \frac{2}{L})]^2}.$$

Collecting these terms, the rate at which the number density of daughter tillers changes over time is equal to the birth of daughter tillers less the maturation into parent tillers and death. Mathematically,

$$\frac{d\, D(t)}{dt} = \underbrace{-\beta\, D(t)}_{\text{death}} + \underbrace{\frac{A^2\, L\, P(t)}{C^2 + [S(t)\, P(t)]^2}}_{\text{births}} - \underbrace{\frac{A^2 L\, P(t - \frac{2}{L})\, \exp(\frac{-2\beta}{L})}{C^2 + [S(t - \frac{2}{L})\, P(t - \frac{2}{L})]^2}}_{\text{maturation}}.$$

The change in parent tiller numbers is governed by the maturation of daughter tillers into parent tillers and the death of parent tillers. Note that the birth of daughter tillers from the parent tiller pool does not deplete the parent pool (denoted by dashed line in Figure 3.2). The rate of maturation of daughter tillers into parent tillers is exactly as shown earlier.

Since a parent tiller produces a finite number of leaves in its lifetime, the death rate of parent tillers depends on the leaf appearance rate. The simplest dependence is linear and this gives the death rate of parent tillers as

$$\alpha L P(t).$$

The rate at which the number density of parent tillers changes over time is equal to the number of daughters maturing into parents less the number of deaths of parent tillers. This is given mathematically by

$$\frac{dP(t)}{dt} = \underbrace{-\alpha L P(t)}_{\text{death}} + \underbrace{\frac{A^2 L P(t-\frac{2}{L}) \exp(\frac{-2\beta}{L})}{C^2 + [S(t-\frac{2}{L}) P(t-\frac{2}{L})]^2}}_{\text{maturation}}.$$

The increase in average parent tiller size, S, is described by the well-known logistic equation

$$\frac{dS(t)}{dt} = r S(t) \left(1 - \frac{S(t)}{S_m}\right)$$

where S_m is the maximum size of a parent tiller and the parameter r is the specific growth rate when S is much smaller than S_m. By the technique of separation of variables, this can be solved exactly, and

$$S(t) = \frac{S_m}{(S_m/S_0 - 1)e^{-rt} + 1}$$

where $S_0 = S(0)$. The relative size of daughter tillers is very small and is neglected by assuming that their size is zero.

Assembling the equations which describe the change in daughter and parent tiller number densities (m^{-2}) and the average size of parent tillers (g) over time gives the following set of ordinary differential equations:

$$\frac{dP(t)}{dt} = -\alpha L P(t) + \frac{A^2 L P(t-\frac{2}{L}) \exp(\frac{-2\beta}{L})}{C^2 + [S(t-\frac{2}{L}) P(t-\frac{2}{L})]^2} \quad (3.1)$$

$$\frac{dD(t)}{dt} = -\beta D(t) + \frac{A^2 L P(t)}{C^2 + [S(t) P(t)]^2} - \frac{A^2 L P(t-\frac{2}{L}) \exp(\frac{-2\beta}{L})}{C^2 + [S(t-\frac{2}{L}) P(t-\frac{2}{L})]^2} \quad (3.2)$$

$$\frac{dS(t)}{dt} = r S(t) \left(1 - \frac{S(t)}{S_m}\right). \quad (3.3)$$

The parameter definitions and estimates are given in Table 3.1.

Parameter	*Biological meaning*	*Estimated value*
α	death proportion of parent tillers	0.075
β	death rate of daughter tillers	0.005 day^{-1}
L	leaf appearance rate	0.03–0.14 day^{-1}
A	$(\frac{A}{C})^2$ is the likelihood of birth of daughter tiller from parent tiller when "mass" of parent tillers is zero	190 g m^{-2}
C	parent tiller "mass" at which births of daughters from parent tillers is decreasing most rapidly	200 g m^{-2}
S_m	maximum size of parent tiller	0.2 g
r	specific growth rate of parent tiller size when size is much smaller than maximum	0.462 * L day^{-1}

Table 3.1: Parameter values for tiller-based grass model

3.2 Numerical solutions

The set of ordinary differential equations (3.1)–(3.3) was solved numerically using a fourth and fifth order Runge-Kutta ODE solver in MATLAB. This was modified

so that it could be used to solve a system of equations which included delay terms.

The initial conditions were chosen as follows:

$$\begin{aligned} P(0) &= 200 \text{ m}^{-2} \\ D(0) &= 500 \text{ m}^{-2} \\ S(0) &= 0.02 \text{ g} \end{aligned}$$

and for $\frac{-2}{L} < t \leq 0$,

$$\begin{aligned} P(t) &= P(0) \\ S(t) &= S(0). \end{aligned}$$

The results obtained by running this model are shown in Figure 3.4. It shows the tiller density of both parent and daughter tillers over 1000 days. Both tiller densities have reached constant values.

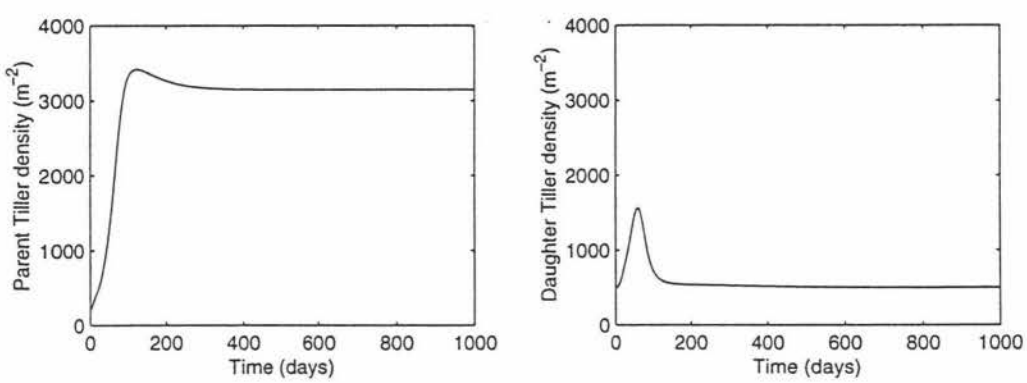

Figure 3.4: Plot of parent tiller density and daughter tiller density vs time

Plotting daughter tiller density against parent tiller density gives Figure 3.5. In this figure, t=0 is denoted by 'o', and every successive 60 days is represented by a '+'. The maximum number density of daughter tillers is at approximately 60 days (seen at the first '+'). Similarly, the number density of parent tillers reaches

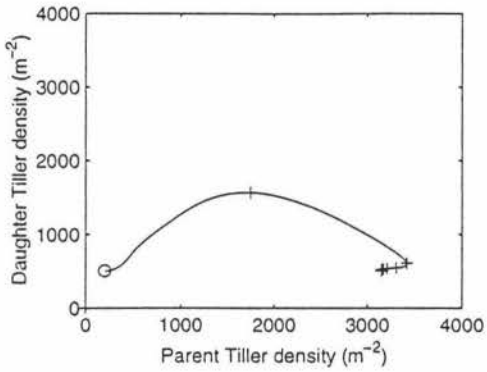

Figure 3.5: Projection of trajectories of tiller-based grass model

a maximum at approximately 120 days. The rate of change then becomes very small, shown by the convergence of '+', again illustrating that steady state values are being reached. This motivated a stability analysis of this steady state, described in the next section.

3.3 Steady States and Stability

3.3.1 Nondimensional Model

To simplify the algebra involved in the analysis of the steady states, it is useful to perform a nondimensionalisation of Equations (3.1)–(3.3). This was done by choosing

$$\tau = tL$$

as a dimensionless time, and scaling parameters so that Equations (3.1)–(3.3) become

$$\frac{d\,\bar{P}(\tau)}{d\tau} = -\alpha\,\bar{P}(\tau) + \frac{\bar{a}^2\,\bar{P}(\tau-2)\,e^{-2\hat{\beta}}}{\bar{c}^2 + [s(\tau-2)\,\bar{P}(\tau-2)]^2} \tag{3.4}$$

$$\frac{d\,\bar{D}(\tau)}{d\tau} = -\hat{\beta}\,\bar{D}(\tau) + \frac{\bar{a}^2\,\bar{P}(\tau)}{\bar{c}^2 + \left[s(\tau)\,\bar{P}(\tau)\right]^2} - \frac{\bar{a}^2\,\bar{P}(\tau-2)\,e^{-2\hat{\beta}}}{\bar{c}^2 + [s(\tau-2)\,\bar{P}(\tau-2)]^2} \tag{3.5}$$

$$\frac{ds(\tau)}{d\tau} = \hat{r}\,s(\tau)\,(1 - s(\tau)) \tag{3.6}$$

where

- lowercase denotes division by S_m (e.g. $a = A/S_m$)
- $\hat{}$ denotes division by L (e.g. $\hat{\beta} = \beta/L$)
- $\bar{}$ denotes division by $P_0 = P(0)$ (e.g. $\bar{c} = c/P_0 = C/(S_m P_0)$).

3.3.2 Steady States

The steady states[1] of the system of Equations (3.4)–(3.6) are found by setting all the time derivatives to zero and solving for the steady states.

From Equation (3.6) there are two steady state values for s, namely $s_{ss} = 0$ and $s_{ss} = 1$. Since a size $s = 0$ for a tiller is not biologically sensible, only the steady state $s_{ss} = 1$ is considered in this analysis. Substituting $s_{ss} = 1$ into the other equations, and then solving for the steady states, two possible values are obtained.

Let $(\bar{P},\ \bar{D},\ s)_{ss}$ represent the steady states of the nondimensional system. The steady states are:

(i) an 'extinct' state

$$\left(\bar{P},\ \bar{D},\ s\right)_{ss} = (0, 0, 1) \tag{3.7}$$

and

(ii) a 'finite' state

$$\left(\bar{P}^*,\ \frac{\alpha}{\hat{\beta}}[e^{2\hat{\beta}} - 1]\bar{P}^*,\ 1\right) \tag{3.8}$$

where

$$\bar{P}^* = \left[\frac{\bar{a}^2}{\alpha}\, e^{-2\hat{\beta}} - \bar{c}^2\right]^{\frac{1}{2}}. \tag{3.9}$$

[1] denoted by $_{ss}$

3.3.3 Local Stability

In the local stability analysis of these steady states, linear systems are obtained by considering a small perturbation from these steady states. Since these perturbations are assumed to be very small, any nonlinear combinations of them can be neglected, and the linear systems are of the form

$$\frac{d\mathbf{x}}{d\tau} = \mathbf{A}\mathbf{x}(\tau) + \mathbf{B}\mathbf{x}(\tau - 2) \tag{3.10}$$

where the perturbation variables are

$$\mathbf{x}(\tau) = \begin{bmatrix} \bar{P}(\tau) - \bar{P}_{ss} \\ \bar{D}(\tau) - \bar{D}_{ss} \\ s(\tau) - s_{ss} \end{bmatrix} = \begin{bmatrix} \pi(\tau) \\ \delta(\tau) \\ \sigma(\tau) \end{bmatrix}$$

and $\mathbf{A}$ and $\mathbf{B}$ are 3×3 matrices with constant entries.

Assuming solutions of the form

$$\mathbf{x} = \mathbf{k}e^{\lambda\tau} \qquad \text{where } \mathbf{k} \text{ is a constant vector,}$$

substituting into Equation (3.10),

$$\begin{aligned} \Rightarrow \quad \lambda\mathbf{k}e^{\lambda\tau} &= \mathbf{A}\mathbf{k}e^{\lambda\tau} + \mathbf{B}\mathbf{k}e^{\lambda(\tau-2)} \\ \Rightarrow \quad \lambda\mathbf{k} &= \mathbf{A}\mathbf{k} + \mathbf{B}e^{-2\lambda}\mathbf{k} \\ \text{or} \quad (\mathbf{A} &+ \mathbf{B}e^{-2\lambda} - \lambda\mathbf{I})\mathbf{k} = 0. \end{aligned}$$

There are nonzero solutions for $\mathbf{k}$ only if λ satisfies the characteristic equation

$$\det[\mathbf{A} + \mathbf{B}e^{-2\lambda} - \lambda\mathbf{I}] = 0.$$

If all the eigenvalues have negative real parts then all solutions are decaying with time, and therefore the steady state is locally stable.

Stability of 'extinct' steady state

Linearisation of the system around $(\bar{P}, \bar{D}, s)_{ss} = (0, 0, 1)$, by considering a perturbation $(\pi, \delta, 1 + \sigma)$ where π, δ and σ are very small, gives

$$\frac{d\pi(\tau)}{d\tau} = -\alpha\pi(\tau) + \frac{\bar{a}^2}{\bar{c}^2}e^{-2\hat{\beta}}\pi(\tau - 2) \tag{3.11}$$

$$\frac{d\delta(\tau)}{d\tau} = -\hat{\beta}\,\delta(\tau) + \frac{\bar{a}^2}{\bar{c}^2}\pi(\tau) - \frac{\bar{a}^2}{\bar{c}^2}e^{-2\hat{\beta}}\,\pi(\tau-2) \tag{3.12}$$

$$\frac{d\,\sigma(\tau)}{d\,\tau} = -\hat{r}\,\sigma(\tau). \tag{3.13}$$

In this linearised system the equations for $\pi(\tau)$ and $\sigma(\tau)$ are completely uncoupled.

Equations (3.11)–(3.13) can be written as

$$\frac{d\mathbf{x}}{d\tau} = \begin{bmatrix} -\alpha & 0 & 0 \\ \frac{\bar{a}^2}{\bar{c}^2} & -\hat{\beta} & 0 \\ 0 & 0 & -\hat{r} \end{bmatrix} \mathbf{x}(\tau) + \begin{bmatrix} \frac{\bar{a}^2}{\bar{c}^2}e^{-2\hat{\beta}} & 0 & 0 \\ -\frac{\bar{a}^2}{\bar{c}^2}e^{-2\hat{\beta}} & 0 & 0 \\ 0 & 0 & 0 \end{bmatrix} \mathbf{x}(\tau-2).$$

The characteristic equation is

$$\det \begin{bmatrix} -\alpha + (\frac{\bar{a}}{\bar{c}})^2 e^{-2(\hat{\beta}+\lambda)} - \lambda & 0 & 0 \\ (\frac{\bar{a}}{\bar{c}})^2[1 - e^{-2(\hat{\beta}+\lambda)}] & -\hat{\beta} - \lambda & 0 \\ 0 & 0 & -\hat{r} - \lambda \end{bmatrix} = 0$$

which simplifies to

$$(\hat{r}+\lambda)(\hat{\beta}+\lambda)\left(-\alpha + (\frac{\bar{a}}{\bar{c}})^2 e^{-2(\hat{\beta}+\lambda)} - \lambda\right) = 0.$$

The eigenvalues are $\lambda = -\hat{r}$, $-\hat{\beta}$ and solutions of Equation (3.14).

$$\lambda + \alpha = \frac{\bar{a}^2}{\bar{c}^2}e^{-2(\hat{\beta}+\lambda)}. \tag{3.14}$$

An interesting feature of delay equations is that their characteristic equations are transcendental and generally will have an infinite number of solutions. It is necessary to look at solutions to Equation (3.14) for λ real and complex.

Let $\lambda = u + iv$. Substituting this into Equation (3.14) and equating real and imaginary parts gives

$$u = -\alpha + (\frac{\bar{a}}{\bar{c}})^2 e^{-2(\hat{\beta}+u)}\cos 2v \tag{3.15}$$

$$v = -(\frac{\bar{a}}{\bar{c}})^2 e^{-2(\hat{\beta}+u)}\sin 2v. \tag{3.16}$$

From Equation (3.16) if v is a solution then so is $-v$, so take $v > 0$ without any loss of generality.

(i) λ real ($v = 0$)

$v = 0$ is a solution to Equation (3.16), and Equation (3.15) becomes

$$u = -\alpha + (\frac{\bar{a}}{\bar{c}})^2 e^{-2(\hat{\beta}+u)}.$$

Let $f(u) = u$ and $g(u) = -\alpha + (\frac{\bar{a}}{\bar{c}})^2 e^{-2(\hat{\beta}+u)}$.

Note that $g'(u) = -2(\frac{\bar{a}}{\bar{c}})^2 e^{-2(\hat{\beta}+u)} < 0$ for all u so $g(u)$ is monotonic decreasing with u. The graphs of $f(u)$ and $g(u)$ are shown in Figure 3.6 for

(a) $g(0) > 0 \Rightarrow -\alpha + (\frac{\bar{a}}{\bar{c}})^2 e^{-2\hat{\beta}} > 0$

(b) $g(0) < 0 \Rightarrow -\alpha + (\frac{\bar{a}}{\bar{c}})^2 e^{-2\hat{\beta}} < 0.$

The intersection of $f(u)$ and $g(u)$ occurs at negative u when $g(0) < 0$, i.e. when

$$\alpha > (\frac{\bar{a}}{\bar{c}})^2 e^{-2\hat{\beta}}.$$

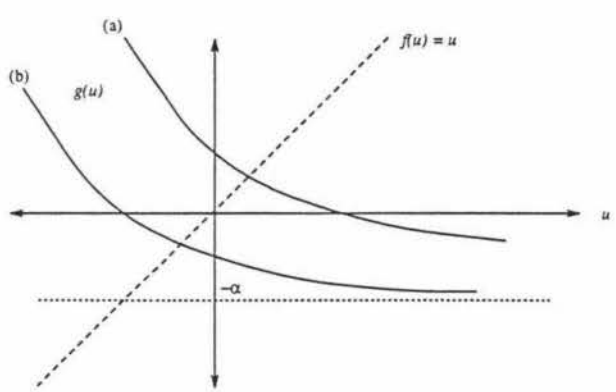

Figure 3.6: λ real for 'extinct' state

(ii) λ complex

Consider Equation (3.16). Let

$$f(v) = v$$

and

$$g(v) = -\left(\frac{\bar{a}}{\bar{c}}\right)^2 e^{-2(\hat{\beta}+u)} \sin 2v.$$

Assume $u > 0$ and look for solutions to (3.16).

Since $\left(\frac{\bar{a}}{\bar{c}}\right)^2$ is a proportion, then

$$0 < \left(\frac{\bar{a}}{\bar{c}}\right)^2 < 1$$

$$\begin{aligned} \Rightarrow \quad 0 \quad < \quad \left(\tfrac{\bar{a}}{\bar{c}}\right)^2 e^{-2(\hat{\beta}+u)} \quad &< \quad e^{-2(\hat{\beta}+u)} \\ &< \quad e^{-2\hat{\beta}}, \qquad \text{if } u > 0 \\ &< \quad 1, \qquad \text{since } \hat{\beta} > 0. \end{aligned}$$

Multiplying through by -1 gives

$$0 > -\left(\frac{\bar{a}}{\bar{c}}\right)^2 e^{-2(\hat{\beta}+u)} > -1.$$

Looking at the graph of $-\sin 2v$, (Figure 3.7), shows that there are no nonzero solutions to Equation (3.16) for v, since $|g(v)| < |\sin 2v|$.

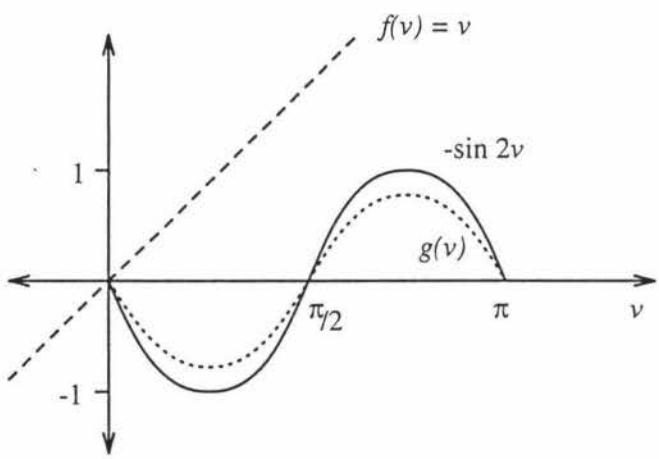

Figure 3.7: Graph of v against $-\sin 2v$

A sufficient but not necessary condition that this steady state be stable is that

$$\alpha > (\frac{\bar{a}}{\bar{c}})^2 e^{-2\hat{\beta}}.$$

However, for typical values of the parameters α, $\bar{a}$, $\bar{c}$ and $\hat{\beta}$, the above inequality does not hold and the 'extinct' steady state is locally unstable.

Stability of 'finite' steady state

Linearisation around the 'finite' steady state given in equation (3.8) gives the following system of equations:

$$\begin{aligned}
\frac{d\pi(\tau)}{d\tau} &= -\alpha\pi(\tau) + \alpha\left[2\alpha\frac{\bar{c}^2}{\bar{a}^2}e^{2\hat{\beta}} - 1\right]\pi(\tau-2) \\
&\quad - 2\bar{a}\alpha^{1/2}e^{-\hat{\beta}}\left[1-\alpha\frac{\bar{c}^2}{\bar{a}^2}e^{2\hat{\beta}}\right]^{\frac{3}{2}}\sigma(\tau-2) \qquad (3.17)\\
\frac{d\delta(\tau)}{d\tau} &= \alpha\left[2\alpha\frac{\bar{c}^2}{\bar{a}^2}e^{2\hat{\beta}} - 1\right]\left[e^{2\hat{\beta}}\pi(\tau) - \pi(\tau-2)\right] - \hat{\beta}\,\delta(\tau) \\
&\quad -2\bar{a}\alpha^{\frac{1}{2}}e^{-\hat{\beta}}\left[1-\alpha\frac{\bar{c}^2}{\bar{a}^2}e^{2\hat{\beta}}\right]^{\frac{3}{2}}\left[e^{2\hat{\beta}}\sigma(\tau) - \sigma(\tau-2)\right] \qquad (3.18)\\
\frac{d\sigma(\tau)}{d\tau} &= -\hat{r}\,\sigma(\tau). \qquad (3.19)
\end{aligned}$$

This can be written as

$$\begin{aligned}
\frac{d\mathbf{x}}{d\tau} &= \begin{bmatrix} -\alpha & 0 & 0 \\ \alpha\, e^{2\hat{\beta}}\left[\frac{2\alpha\bar{c}^2}{\bar{a}^2}e^{2\hat{\beta}} - 1\right] & -\hat{\beta} & -2\bar{a}\alpha^{\frac{1}{2}}e^{\hat{\beta}}\left[1-\frac{\alpha\bar{c}^2}{\bar{a}^2}e^{2\hat{\beta}}\right]^{\frac{3}{2}} \\ 0 & 0 & -\hat{r} \end{bmatrix}\mathbf{x}(\tau) \\
&+ \begin{bmatrix} \alpha\left[\frac{2\alpha\bar{c}^2}{\bar{a}^2}e^{2\hat{\beta}} - 1\right] & 0 & -2\bar{a}\alpha^{\frac{1}{2}}e^{-\hat{\beta}}\left[1-\frac{\alpha\bar{c}^2}{\bar{a}^2}e^{2\hat{\beta}}\right]^{\frac{3}{2}} \\ -\alpha\left[\frac{2\alpha\bar{c}^2}{\bar{a}^2}e^{2\hat{\beta}} - 1\right] & 0 & 2\bar{a}\alpha^{\frac{1}{2}}e^{-\hat{\beta}}\left[1-\frac{\alpha\bar{c}^2}{\bar{a}^2}e^{2\hat{\beta}}\right]^{\frac{3}{2}} \\ 0 & 0 & 0 \end{bmatrix}\mathbf{x}(\tau-2).
\end{aligned}$$

The characteristic equation is

$$\det\begin{bmatrix} -\alpha + \alpha\left[\frac{2\alpha\bar{c}^2}{\bar{a}^2}e^{2\hat{\beta}}-1\right]e^{-2\lambda} - \lambda & 0 & -2\bar{a}\alpha^{\frac{1}{2}}e^{-\hat{\beta}}\left[1-\frac{\alpha\bar{c}^2}{\bar{a}^2}e^{2\hat{\beta}}\right]^{\frac{3}{2}}e^{-2\lambda} \\ \alpha\left[\frac{2\alpha\bar{c}^2}{\bar{a}^2}e^{2\hat{\beta}}-1\right](e^{2\hat{\beta}}-e^{-2\lambda}) & -\hat{\beta}-\lambda & -2\bar{a}\alpha^{\frac{1}{2}}e^{-\hat{\beta}}\left[1-\frac{\alpha\bar{c}^2}{\bar{a}^2}e^{2\hat{\beta}}\right]^{\frac{3}{2}}(e^{2\hat{\beta}}-e^{-2\lambda}) \\ 0 & 0 & -\hat{r}-\lambda \end{bmatrix} = 0$$

which simplifies to

$$(\hat{\beta}+\lambda)(\hat{r}+\lambda)\left(-\alpha + \alpha\left[\frac{2\alpha\bar{c}^2}{\bar{a}^2}e^{2\hat{\beta}} - 1\right]e^{-2\lambda} - \lambda\right) = 0.$$

Two eigenvalues are $\lambda = -\hat{\beta}, -\hat{r}$. The other eigenvalues are found by solving

$$\alpha + \lambda = \left[\frac{2\alpha\bar{c}^2}{\bar{a}^2}e^{2\hat{\beta}} - 1\right]\alpha e^{-2\lambda}. \qquad (3.20)$$

Putting $\lambda = u + iv$, substituting into Equation (3.20), and equating real and imaginary parts gives

$$u = -\alpha + \left[\frac{2\alpha\bar{c}^2}{\bar{a}^2}e^{2\hat{\beta}} - 1\right]\alpha e^{-2u}\cos 2v \tag{3.21}$$

$$v = -\left[\frac{2\alpha\bar{c}^2}{\bar{a}^2}e^{2\hat{\beta}} - 1\right]\alpha e^{-2u}\sin 2v. \tag{3.22}$$

Again note that if v is a solution to Equation (3.22) then so is $-v$, so take $v > 0$ without loss of generality.

(i) λ real. $(v = 0)$

$v = 0$ is a solution to Equation (3.22), and Equation (3.21) becomes

$$u = -\alpha + \left[\frac{2\alpha\bar{c}^2}{\bar{a}^2}e^{2\hat{\beta}} - 1\right]\alpha e^{-2u}.$$

Let $f(u) = u$ and $g(u) = -\alpha + \left[\frac{2\alpha\bar{c}^2}{\bar{a}^2}e^{2\hat{\beta}} - 1\right]\alpha e^{-2u}$. Note that the slope of $g(u)$ depends on the sign of $\frac{2\alpha\bar{c}^2}{\bar{a}^2}e^{2\hat{\beta}} - 1$ so look at each case separately.

(a) $\frac{2\alpha\bar{c}^2}{\bar{a}^2}e^{2\hat{\beta}} - 1 > 0$

Clearly,

$$g'(u) = -2\left[\frac{2\alpha\bar{c}^2}{\bar{a}^2}e^{2\hat{\beta}} - 1\right]\alpha e^{-2u} < 0$$

for all u, and Figure 3.8a shows a similar argument to the 'extinct' steady state. Namely, $f(u) = g(u)$ for $u < 0$ when $g(0) < 0$, leading to the inequality

$$\alpha < \frac{\bar{a}^2}{\bar{c}^2}e^{-2\hat{\beta}}.$$

(b) $\frac{2\alpha\bar{c}^2}{\bar{a}^2}e^{2\hat{\beta}} - 1 < 0$

In this case, $g'(u) > 0$ for all u, and in fact $g(u) < -\alpha$ for all u. Figure 3.8b shows that any solution to $f(u) = g(u)$ will be for $u < 0$.

Therefore, λ is negative when

$$\alpha < \frac{\bar{a}^2}{\bar{c}^2}e^{-2\hat{\beta}}$$

which is also the condition required for this steady state to exist (Equation 3.9).

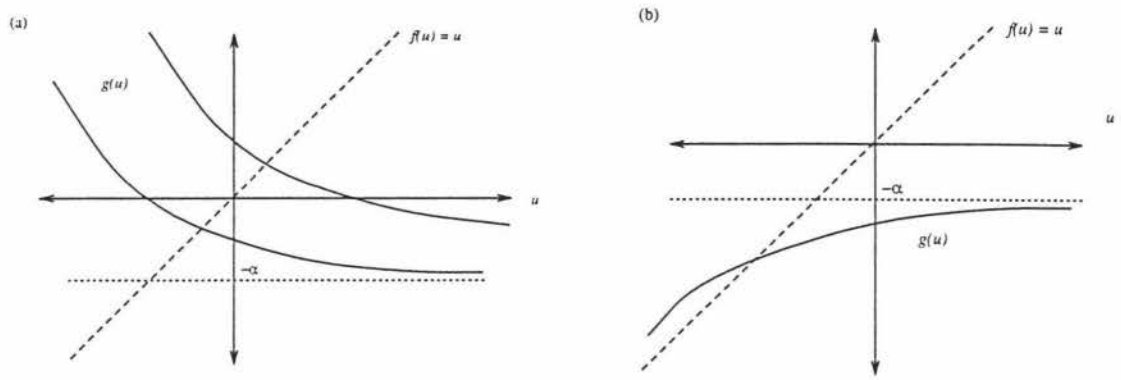

Figure 3.8: λ real for 'finite' state

(ii) λ complex. ($v \neq 0$)

Consider Equation (3.22). Let

$$f(v) = v$$

and

$$g(v) = -\left[\frac{2\alpha\bar{c}^2}{\bar{a}^2}e^{2\hat{\beta}} - 1\right]\alpha e^{-2u}\sin 2v.$$

First look at the solutions to (3.22) for v on the assumption that $u > 0$.

For existence of the 'finite' steady state, it is required that

$$\begin{aligned} & 0 < \alpha\tfrac{\bar{c}}{\bar{a}}^2 e^{2\hat{\beta}} < 1 \\ \Rightarrow \quad & 0 < 2\alpha\tfrac{\bar{c}}{\bar{a}}^2 e^{2\hat{\beta}} < 2 \\ \Rightarrow \quad & -1 < \left[2\alpha\tfrac{\bar{c}}{\bar{a}}^2 e^{2\hat{\beta}} - 1\right] < 1. \end{aligned}$$

Consider the two cases

$$\begin{aligned} \text{(a)} \quad & 0 < \left[2\alpha\tfrac{\bar{c}}{\bar{a}}^2 e^{2\hat{\beta}} - 1\right] < 1 \\ \text{(b)} \quad & -1 < \left[2\alpha\tfrac{\bar{c}}{\bar{a}}^2 e^{2\hat{\beta}} - 1\right] < 0. \end{aligned}$$

(a) If $0 < \left[2\alpha\frac{\bar{c}}{\bar{a}}^2 e^{2\hat{\beta}} - 1\right] < 1$ then

$$\begin{aligned} 0 < \left[2\alpha\tfrac{\bar{c}}{\bar{a}}^2 e^{2\hat{\beta}} - 1\right]\alpha e^{-2u} &< \alpha e^{-2u} \\ &< \alpha, \qquad \text{if } u > 0 \\ &< 1, \qquad \text{since } \alpha \text{ is a proportion} \end{aligned}$$

$$\text{and} \quad -1 < -\left[2\alpha\tfrac{\bar{c}}{\bar{a}}^2 e^{2\hat{\beta}} - 1\right]\alpha e^{-2u} < 0.$$

Thus, $g(v)$ is a sine function $g(v) = \kappa \sin 2v$ where $-1 < \kappa < 0$. Figure 3.7 shows that there are no nonzero solutions for v, since $|g(v)| < |\sin 2v|$.

(b) $-1 < \left[2\alpha\frac{\bar{c}}{\bar{a}}^2 e^{2\hat{\beta}} - 1\right] < 0$

Since

$$\begin{aligned} 2\alpha(\tfrac{\bar{c}}{\bar{a}})^2 e^{2\hat{\beta}} - 1 &< 0 \\ \Rightarrow \quad 2\alpha &< (\tfrac{\bar{a}}{\bar{c}})^2 e^{-2\hat{\beta}} \\ &< e^{-2\hat{\beta}} \qquad \text{since } \tfrac{\bar{a}}{\bar{c}} \text{ is a proportion} \\ &< 1 \qquad \text{since } \hat{\beta} > 0 \\ \Rightarrow \quad \alpha &< \tfrac{1}{2}. \end{aligned}$$

Now, if

$$\begin{aligned} -1 < \left[2\alpha\tfrac{\bar{c}}{\bar{a}}^2 e^{2\hat{\beta}} - 1\right] &< 0 \\ \Rightarrow \quad 1 > \left[1 - 2\alpha(\tfrac{\bar{c}}{\bar{a}})^2 e^{2\hat{\beta}}\right] &> 0 \\ \Rightarrow \quad 0 < \left[1 - 2\alpha(\tfrac{\bar{c}}{\bar{a}})^2\right]\alpha e^{-2u} &< \alpha e^{-2u} \\ \Rightarrow \quad 0 < \left[1 - 2\alpha(\tfrac{\bar{c}}{\bar{a}})^2\right]\alpha e^{-2u} &< \tfrac{1}{2}e^{-2u} \quad \text{(from above)} \\ \Rightarrow \quad 0 < \left[1 - 2\alpha(\tfrac{\bar{c}}{\bar{a}})^2\right]\alpha e^{-2u} &< \tfrac{1}{2} \qquad \text{if } u > 0. \end{aligned}$$

Thus $g(v)$ lies under the graph of $\frac{1}{2}\sin 2v$. The derivative of $\frac{1}{2}\sin 2v$ is $\cos 2v$, so the slope at $v = 0$ is 1. As v increases, the slope decreases, so the only intersection is at $v = 0$ as shown in Figure 3.9.

Thus, if $u > 0$ there are no nonzero solutions of Equation (3.22).

From (3.21) and (3.22)

$$u = -(\alpha + v \cot 2v).$$

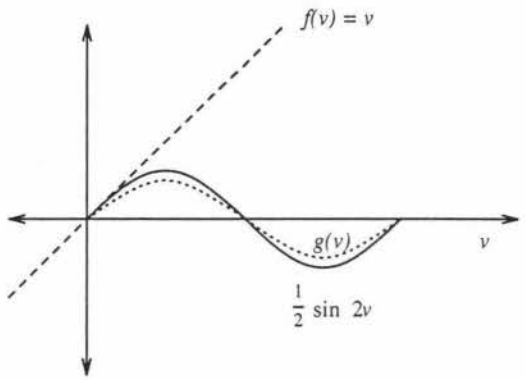

Figure 3.9: Graph of v against $\frac{1}{2}\sin 2v$

Substituting into (3.22) gives

$$v = -\left[\frac{2\alpha\bar{c}^2}{\bar{a}^2}e^{2\hat{\beta}} - 1\right]\alpha e^{2(\alpha+v\cot 2v)}\sin 2v. \tag{3.23}$$

The assumption that $u > 0$ leads to the conclusion that (3.22) has no solutions. Hence any solutions of Equation (3.23) must correspond to $u < 0$. Therefore, if λ is complex then $\Re(\lambda) < 0$.

The inequality that ensures the real part of λ is negative,

$$\alpha < \frac{\bar{a}^2}{\bar{c}^2}e^{-2\hat{\beta}},$$

is precisely the condition that the 'finite' steady state exists. Therefore, if this 'finite' steady state exists, it is locally stable.

Bifurcation Graph

The stability of the steady states can be shown graphically, on a bifurcation graph. Let

$$\xi = -\alpha + \left(\frac{\bar{a}}{\bar{c}}\right)^2 e^{-2\hat{\beta}}.$$

Figure 3.10 shows the steady state of parent tillers $\bar{P}_{ss}$ plotted against ξ. This demonstrates that when $\xi \leq 0$, the only steady state is $\bar{P}_{ss} = 0$ which is stable.

When $\xi > 0$ the steady state $\bar{P}_{ss} = 0$ becomes unstable, and the 'finite' steady state $\bar{P}_{ss} = \bar{P}^*$ is stable.

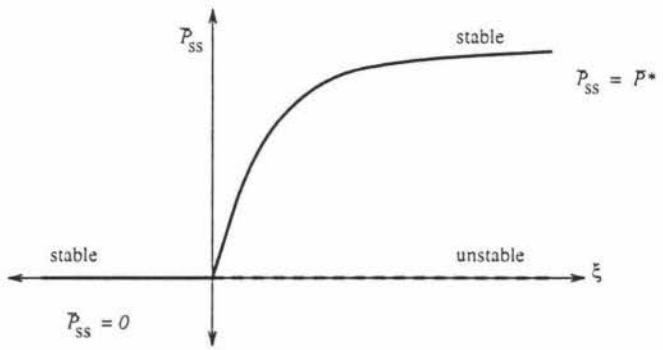

Figure 3.10: Bifurcation diagram for tiller-based grass model

3.4 Global stability

Global stability of a steady state is much more difficult to establish because non-linear terms can no longer be neglected. One option is to compute solutions via the numerical method described in Section 3.2 for various initial numbers of parent and daughter tillers. Figure 3.11 shows convergence of the solution curves towards the 'finite' steady state from three different initial population sizes. An initial size of 0.02 g was used throughout.

The 'finite' steady state appears to be globally stable but numerical simulation cannot prove this as there is an infinite amount of parameter space to be investigated. There must be some parent tillers present initially otherwise, from Equations (3.1) and (3.2), the number of daughter tillers decays exponentially to zero.

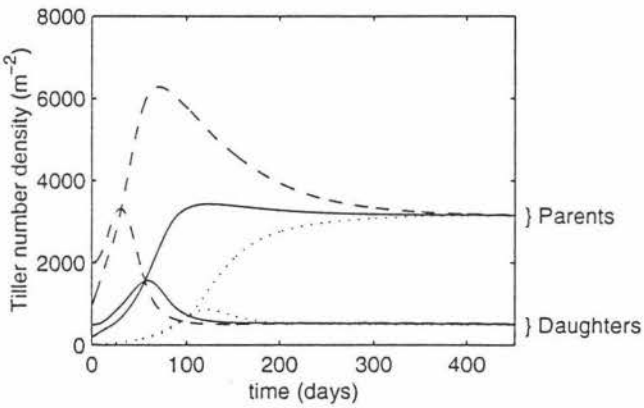

— $P(0) = 200, \quad D(0) = 500,$
– – $P(0) = 1000, \quad D(0) = 2000,$
· · · $P(0) = 20, \quad D(0) = 10.$

Figure 3.11: Tiller number density against time with different initial conditions

3.5 Harvesting

Harvesting was simulated by periodically reducing the size of the parent tillers back to the original size. Figure 3.12 shows the reduction of size with harvesting period of 30 days.

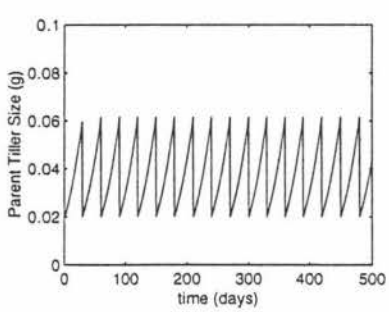

Figure 3.12: Size vs time with 30 day harvest

Since daughter tillers are very small many escape harvesting. However, as a result of harvesting, a small proportion of both parents and daughters may die and this proportion can be set when running the model. The results obtained in Figure 3.13 assume no parent or daughter tillers die when harvesting.

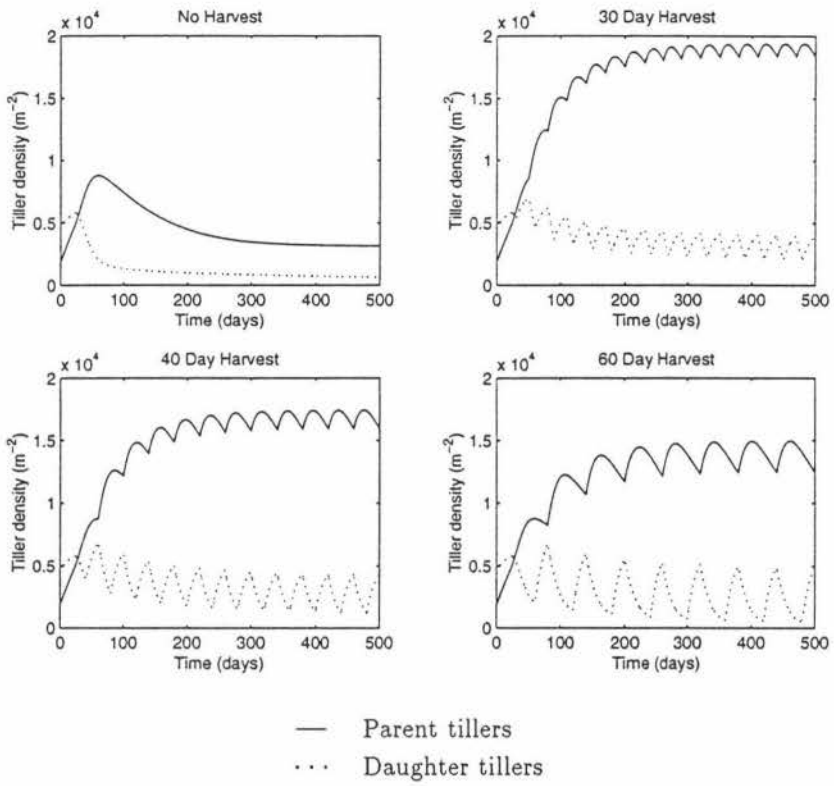

Figure 3.13: Time plots of tiller-based grass model with different harvesting regimes

Figure 3.13 shows the solutions without harvesting and three different harvesting regimes. The harvesting intervals used are thirty days, forty days, and sixty days, respectively. It is evident that the solution curves have reached some limits within which they oscillate. The average tiller density reached is higher in the thirty day harvest than the forty and sixty day harvests. Figure 3.14 shows that the eventual average number of parent tillers decreases as the interval between harvests increases.

It was found that as the frequency of harvesting increases, the average size of parent tillers decreases and the number density increases, i.e. there is an inverse relationship between tiller numbers and the size of parent tillers.

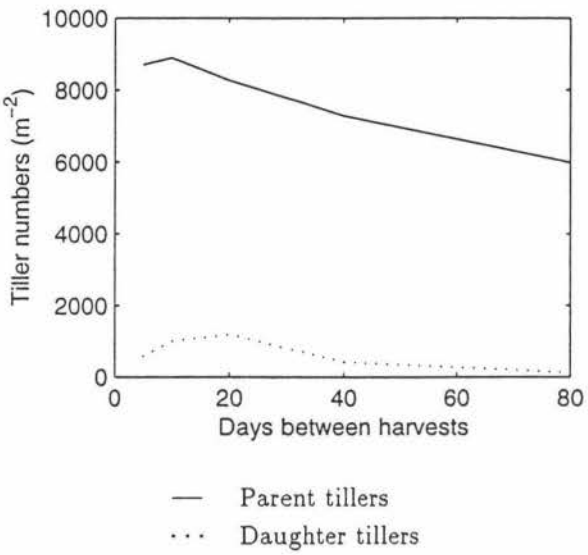

Figure 3.14: Tiller number density just before harvest vs days between harvests

The long-term growth rate (g m^{-2} day^{-1}) is relatively constant over a range of harvesting intervals (10-40 days), as shown in Figure 3.15.

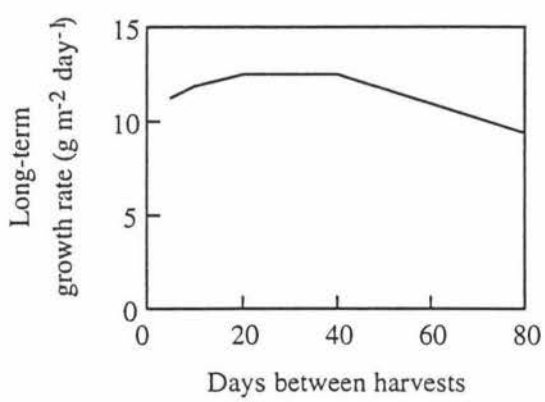

Figure 3.15: Long-term growth rate vs days between harvests

3.6 Summary and comments

This chapter presented a model constructed to describe the growth of ryegrass based on tillering. This model introduced the use of delay to describe the maturation of daughter tillers. The numerical simulations provided solution curves of the model.

An investigation of the steady states of the system of equations showed an 'extinct' steady state and a 'finite' steady state. A condition was found for the existence of the 'finite' steady state. When this condition is satisfied, the 'finite' steady state is locally stable and the 'extinct' steady state is locally unstable. For typical parameters this condition is satisfied.

Establishing the global stability of the steady states is difficult and numerical solutions have been calculated for many different initial conditions. It appears that for all positive nonzero initial conditions the 'finite' steady state is reached.

Harvesting was simulated and it was found that more regular harvesting resulted in higher numbers of smaller tillers.

The model presented in this chapter exhibits similiar behaviour to ryegrass plants growing in the field (H. Clark, personal communication). Typical behaviour includes

1. steady state population number density is reached
2. increased frequency of harvesting results in greater number of parent tillers (See Figure 3.14.)
3. growth rate is relatively constant over a range of harvesting intervals.

Chapter 4

A Growing Point based Clover Model

This chapter investigates two models describing the growth of clover. As described in Section 1.1, a clover plant consists of viable buds, incipient branches and growing points (Figure 4.1).

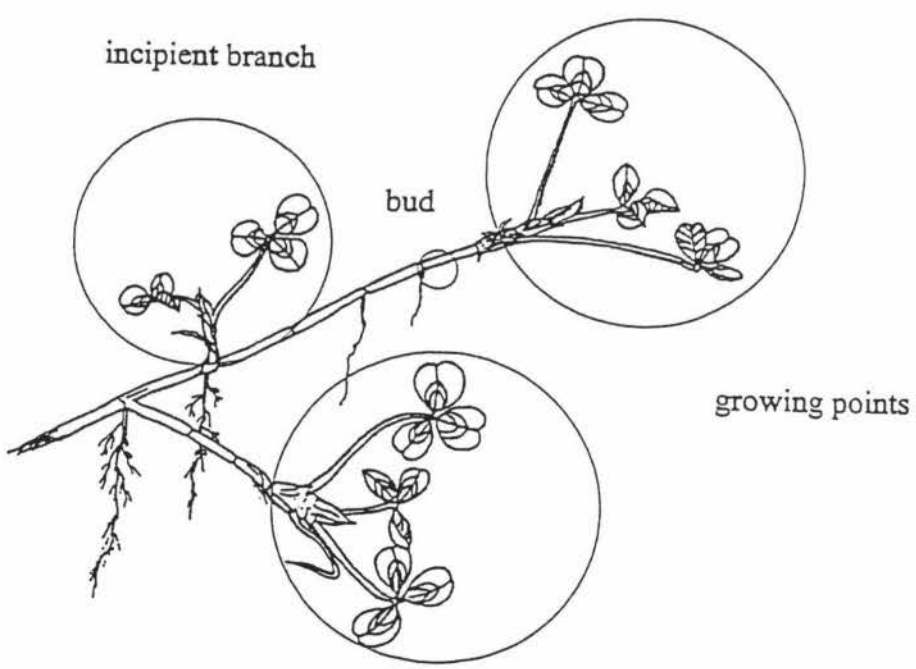

Figure 4.1: A clover plant

4.1 Model Description

The model described by Louie et al. [19], comprises three interacting variables: viable buds (VB), incipient branches (IB), and growing points (GP). Viable buds grow into incipient branches, and these incipient branches become growing points once they have three leaves. Growing points give rise to new viable buds, but this does not decrease the growing point pool size, unlike the transition from viable buds to incipient branches, and incipient branches to growing points which do decrease their source pools. These interactions are shown in Figure 4.2.

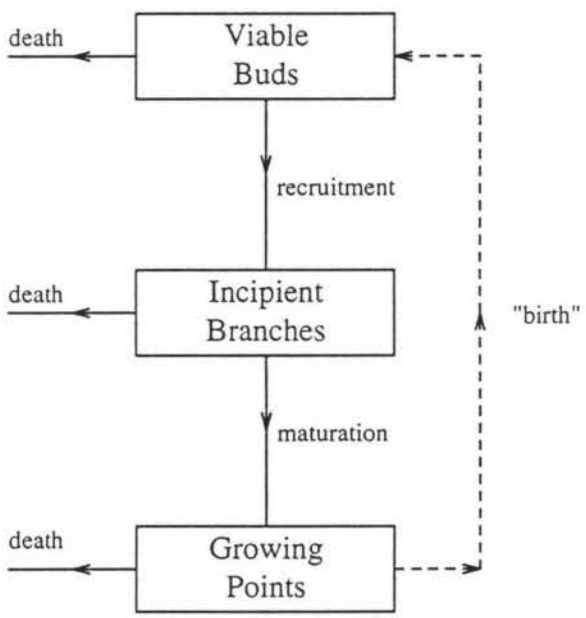

Figure 4.2: Clover model interactions

4.1.1 First Model - *without delay*

Firstly consider the change in numbers of viable buds (Figure 4.2). The change in numbers is dependent on the "birth" of viable buds, recruitment of viable buds into incipient branches and natural death of viable buds.

The recruitment of incipient branches from viable buds is assumed to follow the

same relationship as the "birth" of daughter tillers from parent tillers in the grass model of Chapter 3. The mass density of growing points is defined as the product $S(t)\,GP(t)$. Mathematically the rate at which viable buds develop into incipient branches is

$$\frac{A^2\,b\,VB(t)}{C^2 + [S(t)\,GP(t)]^2}$$

where b is the bud appearance rate, and $(A/C)^2$ is the likelihood of viable buds developing into incipient branches when the growing point mass is zero.

The "birth" of viable buds is taken as a proportion, K, of the growing point population. Mathematically the birth rate of viable buds is

$$K\,b\,GP(t).$$

The number of viable buds which die naturally depends on the bud appearance rate, b. The death rate is given by

$$\alpha\,b\,VB(t).$$

Collecting these terms, the differential equation representing the change in viable bud number density over time is:

$$\frac{dVB(t)}{dt} = \underbrace{K\,b\,GP(t)}_{\text{birth}} - \underbrace{\alpha\,b\,VB(t)}_{\text{death}} - \underbrace{\frac{A^2\,b\,VB(t)}{C^2 + [S(t)\,GP(t)]^2}}_{\text{recruitment}}.$$

Similarly, the change in number density of incipient branches results from the number of viable buds developing into incipient branches, the number of incipient branches maturing into growing points and the natural deaths of incipient branches (Figure 4.2).

Recruitment of incipient branches from viable buds is precisely the term described earlier, i.e.

$$\frac{A^2\, b\, VB(t)}{C^2 + [S(t)\, GP(t)]^2}.$$

The maturation of incipient branches into growing points at time t is assumed to be a proportion, $\frac{1}{3}$, of the incipient branch population at that time. This is because the incipient branch population is assumed to consist of equal numbers of 0, 1 and 2 leaved members. The rate of maturation of incipient branches into growing points is described mathematically as

$$\frac{1}{3} b\, IB(t).$$

The death rate of incipient branches is

$$\delta\, b\, [IB(t)]^{\gamma}$$

where γ is a "shape" parameter whose value is usually taken as one.

Together, these terms describe the rate of change in incipient branch number density over time

$$\frac{d\, IB(t)}{dt} = \underbrace{\frac{A^2\, b\, VB(t)}{C^2 + [S(t)\, GP(t)]^2}}_{\text{recruitment}} - \underbrace{\delta\, b\, [IB(t)]^{\gamma}}_{\text{death}} - \underbrace{\frac{1}{3} b\, IB(t)}_{\text{maturation}}.$$

Finally, the growing point population is governed by natural death of growing points and maturation of incipient branches into growing points. Note that although growing points give rise to viable buds, this does not deplete the growing point population (denoted by dashed line of Figure 4.2). The rate of death of growing points is

$$d\, b\, GP(t)$$

where d is the proportion of growing points dying naturally.

Growing points which have matured from incipient branches is exactly that given above, i.e.

$$\frac{1}{3} b\, IB(t).$$

Collecting these terms, the differential equation describing the rate of change of growing point number density over time is

$$\frac{dGP(t)}{dt} = \underbrace{\frac{1}{3} b\, IB(t)}_{\text{maturation}} - \underbrace{d\, b GP(t)}_{\text{death}}.$$

The differential equation governing the average size of growing points, $S(t)$, is taken as

$$\frac{dS(t)}{dt} = r\, S(t)(1 - S(t)/S_m)$$

where S_m is the maximum size of a growing point and the parameter r is the specific growth rate when S is much smaller than S_m. This is exactly the same differential equation which describes the average size of parent tillers in the grass model of Chapter 3.

The differential equations presented above together constitute the following dynamical system:

$$\frac{dVB(t)}{dt} = K\, b GP(t) - \alpha\, b VB(t) - \frac{A^2\, b VB(t)}{C^2 + [S(t)\, GP(t)]^2} \tag{4.1}$$

$$\frac{dIB(t)}{dt} = \frac{A^2\, b VB(t)}{C^2 + [S(t)\, GP(t)]^2} - \delta\, b[IB(t)]^\gamma - \frac{1}{3} b\, IB(t) \tag{4.2}$$

$$\frac{dGP(t)}{dt} = \frac{1}{3} b\, IB(t) - d\, b GP(t) \tag{4.3}$$

$$\frac{dS(t)}{dt} = r\, S(t)(1 - S(t)/S_m). \tag{4.4}$$

The parameters are defined in Table 4.1.

Parameter	*Biological meaning*	*Estimated value*
b	bud appearance rate	0.05-0.2 day^{-1}
C	growing point "mass" at which flux from viable bud to incipient branch is decreasing most rapidly	100 g m^{-2}
A	$(A/C)^2$ is the likelihood of transition from viable bud to incipient branch when growing point "mass" is zero	95 g m^{-2}
δ	specific death proportion of incipient branches	0.1
γ	"shape" parameter for specific death rate of incipient branches	1
K	the proportion of growing points giving rise to new viable buds	0.7
α	the proportion of viable buds being lost through natural mortality	0.05
d	specific death proportion of growing points	0.08 day^{-1}
r	specific growth rate of growing point size when size is much smaller than maximum	0.4 day^{-1}
S_m	maximum size of individual growing point	0.02 g

Table 4.1: Parameter values for clover model

4.1.2 Second Model - *with delay*

The assumption of equal proportions of 0, 1 and 2 leaved members may not, in practice, be realistic. The model described above was therefore modified to incorporate the delayed regulation of the rate of production of growing points. Instead of assuming that, at every instant in time, a proportion of incipient branches become growing points, the number of viable buds that were "born" two bud appearance intervals ago, at time $(t - \frac{2}{b})$, will determine the number of growing points at time t. Therefore, instead of the rate of maturation being

$$\frac{1}{3} b\, IB(t)$$

it is now described as the rate of incipient branches developing from viable buds evaluated at time $(t - \frac{2}{b})$. This is then scaled by the proportion that actually survive two bud appearance intervals, $e^{-2\delta}$. Thus the term describing the rate of maturation of incipient branches into growing points is

$$\frac{A^2\, b\, VB(t - \frac{2}{b})\, e^{-2\delta}}{C^2 + \left[S(t - \frac{2}{b})\, GP(t - \frac{2}{b})\right]^2}.$$

This term replaces $\frac{1}{3} b\, IB(t)$ in Equations (4.2) and (4.3). The differential equations governing the viable bud number density and average size of growing points are precisely the same as Equation (4.1) and (4.4).

Modifying the first model to account for this delay gives the following system of ordinary differential-delay equations:

$$\frac{dVB(t)}{dt} = K\, b\, GP(t) - \alpha\, b\, VB(t) - \frac{A^2\, b\, VB(t)}{C^2 + [S(t)\, GP(t)]^2} \tag{4.5}$$

$$\begin{aligned}\frac{dIB(t)}{dt} &= \frac{A^2\, b\, VB(t)}{C^2 + [S(t)\, GP(t)]^2} - \delta\, b\, [IB(t)]^{\gamma} \\ &\quad - \frac{A^2\, b\, VB(t - \frac{2}{b})\, e^{-2\delta}}{C^2 + \left[S(t - \frac{2}{b})\, GP(t - \frac{2}{b})\right]^2}\end{aligned} \tag{4.6}$$

$$\frac{dGP(t)}{dt} = \frac{A^2\, b\, VB(t - \frac{2}{b})\, e^{-2\delta}}{C^2 + \left[S(t - \frac{2}{b})\, GP(t - \frac{2}{b})\right]^2} - d\, b\, GP(t) \tag{4.7}$$

$$\frac{dS(t)}{dt} = r\,S(t)\,(1 - S(t)/S_m)\,. \tag{4.8}$$

The size equation (4.4) or (4.8) is uncoupled from the others and is the well-known logistic equation. Its solution is

$$S(t) = \frac{S_m}{(S_m/S_0 - 1)e^{-rt} + 1}$$

where $S_0 = S(0)$.

The parameters are defined in Table 4.1.

4.2 Numerical solutions

A fourth-fifth order Runge-Kutta ODE solver using MATLAB [29] was used to give numerical solutions, and a modification of this used for the model with delay. These simulations were run for 2000 days with initial conditions:

$$\begin{aligned} VB(0) &= 100\,\mathrm{m}^{-2} \\ IB(0) &= 100\,\mathrm{m}^{-2} \\ GP(0) &= 100\,\mathrm{m}^{-2} \\ S(0) &= 0.02\,\mathrm{g} \end{aligned}$$

and for $\frac{-2}{b} < t \leq 0$

$$\begin{aligned} GP(t) &= GP(0) \\ S(t) &= S(0). \end{aligned}$$

Figure 4.3 shows the solution curves for both models where the model without the delay terms is given by the solid lines, and the dotted lines represent the "delayed" solution curves. It is apparent that all three state variables have reached asymptotic values after a long time.

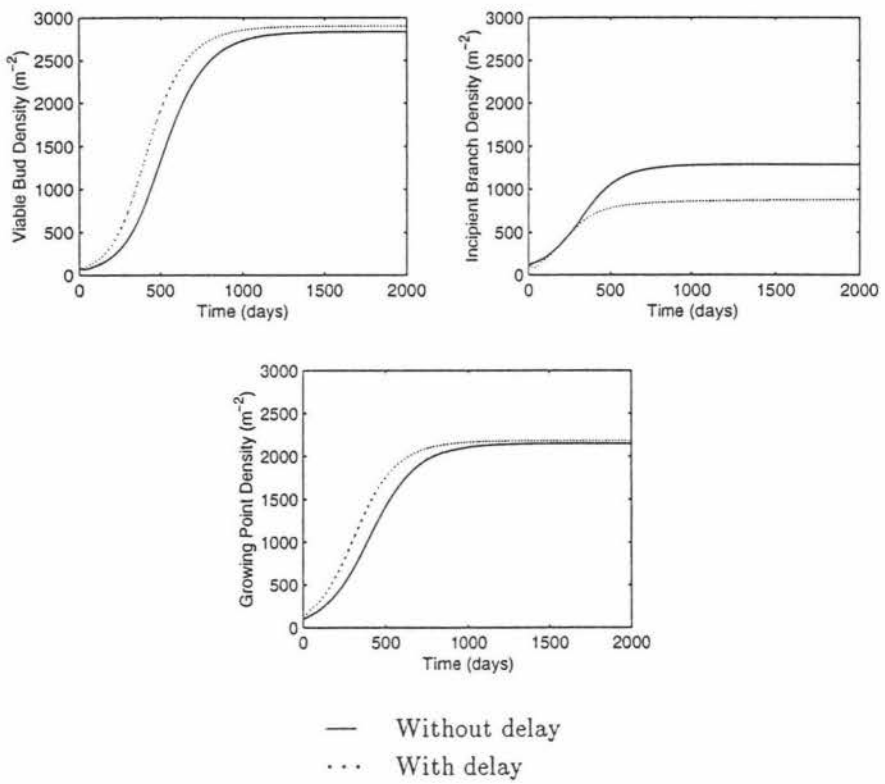

Figure 4.3: Plots of viable bud, incipient branch and growing point number densities vs time

This asymptotic behaviour can also be seen from Figure 4.4 where every 200 days is indicated by '+' (without delay) and '*' (with delay). This motivated an investigation of the steady states of the system, and the stability of these steady states.

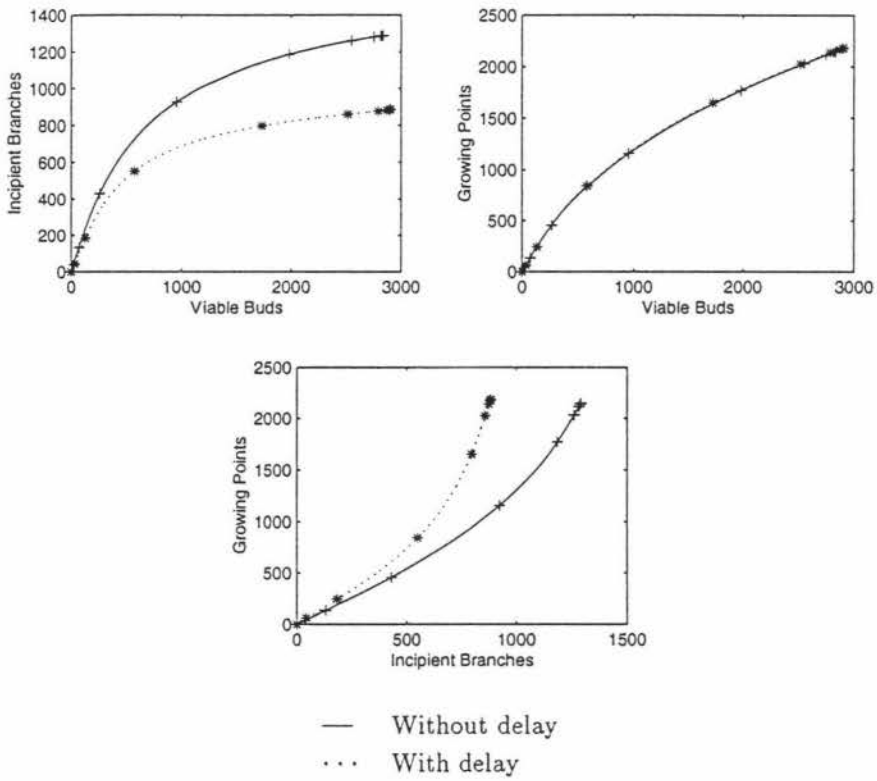

Figure 4.4: Projection of trajectories

4.3 Steady State Analysis

As with the grass model described in Chapter 3, it is useful to express the clover models in nondimensional terms. This was done by choosing

$$\tau = bt$$

as a dimensionless time. The specific growth rate r was scaled by b as follows

$$\hat{r} = \frac{r}{b}.$$

Also, the state variable $S(t)$ was scaled by S_m, and the state variables VB, IB and GP were scaled by the initial value of viable buds $VB(0)$, i.e.

$$\begin{aligned} s(\tau) &= \frac{S(t)}{S_m} \\ V(\tau) &= \frac{VB(t)}{VB(0)} \\ I(\tau) &= \frac{IB(t)}{VB(0)} \\ G(\tau) &= \frac{GP(t)}{VB(0)}. \end{aligned}$$

With these scalings nondimensional parameters a and c are introduced where

$$\begin{aligned} a &= \frac{A}{S_m\, VB(0)} \\ c &= \frac{C}{S_m\, VB(0)}. \end{aligned}$$

4.3.1 Without delay

With this change in variables, the following nondimensional system for equations (4.1)–(4.4) is obtained:

$$\frac{dV(\tau)}{d\tau} = K\,G(\tau) - \alpha\,V(\tau) - \frac{a^2\,V(\tau)}{c^2 + [s(\tau)\,G(\tau)]^2} \tag{4.9}$$

$$\frac{dI(\tau)}{d\tau} = \frac{a^2\,V(\tau)}{c^2 + [s(\tau)\,G(\tau)]^2} - \delta\,[I(\tau)]^\gamma - \frac{1}{3}I(\tau) \tag{4.10}$$

$$\frac{dG(\tau)}{d\tau} = \frac{1}{3}I(\tau) - d\,G(\tau) \tag{4.11}$$

$$\frac{ds(\tau)}{d\tau} = \hat{r}\,s(\tau)(1 - s(\tau)). \tag{4.12}$$

The steady states of the system of Equations (4.9)–(4.12) are found by setting all the time derivatives to zero and solving the resulting algebraic equations. From (4.12) there are two steady state values for s, namely $s_{ss} = 0$ and $s_{ss} = 1$. Since

a size $s = 0$ for a growing point is not biologically sensible, only the steady state $s_{ss} = 1$ is considered in this analysis. Substituting $s_{ss} = 1$ into the other equations, and then solving for the steady states, two possible values are obtained as follows:
(i) an 'extinct' state

$$(V,\ I,\ G,\ s)_{ss} \ = \ (0,\ 0,\ 0,\ 1)$$

and
(ii) a 'finite' state

$$\left(\frac{K(c^2 + G^{*2})\, G^*}{\alpha\,(c^2 + G^{*2}) + a^2},\ 3d\,G^*,\ G^*,\ 1 \right)$$

where G^* satisfies the equation

$$\alpha\,\delta\,(3d)^\gamma\, G^{(\gamma+1)} + \delta\,(3d)^\gamma\,(\alpha\,c^2 + a^2)\, G^{(\gamma-1)} + \alpha\,d\,G^2 + d\,(\alpha\,c^2 + a^2) - a^2 K = 0.$$

For the usual parameter value of $\gamma = 1$, this reduces to a quadratic equation with positive solution

$$G^* \ = \ \left[\frac{K\,a^2}{\alpha\,(3\delta + 1)\,d} - \frac{a^2}{\alpha} - c^2 \right]^{\frac{1}{2}}. \tag{4.13}$$

Note: Neither α nor d can equal zero. (If $\alpha = 0$, this means that no viable buds die; if $d = 0$, then no growing points die. In either case, the clover population will "explode".) It is interesting to note that if the death of incipient branches is zero ($\delta = 0$), a finite steady state is still reached.

Stability of the 'extinct' state

To look at the local stability of the first of these steady states, consider a small perturbation from (0, 0, 0, 1) by putting

$$V = v$$

$$I = i$$

$$G = g$$

$$s = 1 + \sigma$$

where v, i, g, σ are assumed small.

By neglecting all terms of second and higher order, the following linear system is obtained:

$$\frac{dv}{d\tau} = Kg - [\alpha + \frac{a^2}{c^2}]v \tag{4.14}$$

$$\frac{di}{d\tau} = \frac{a^2}{c^2}v - (\delta + \frac{1}{3})i \tag{4.15}$$

$$\frac{dg}{d\tau} = \frac{1}{3}i - dg \tag{4.16}$$

$$\frac{d\sigma}{d\tau} = -\hat{r}\,\sigma. \tag{4.17}$$

This linear system can be written as

$$\frac{d\mathbf{x}}{d\tau} = \mathbf{A}\mathbf{x} \tag{4.18}$$

where

$$\mathbf{x} = \begin{bmatrix} v \\ i \\ g \\ \sigma \end{bmatrix}$$

and

$$\mathbf{A} = \begin{bmatrix} -(\alpha + \frac{a^2}{c^2}) & 0 & K & 0 \\ \frac{a^2}{c^2} & -(\delta + \frac{1}{3}) & 0 & 0 \\ 0 & \frac{1}{3} & -d & 0 \\ 0 & 0 & 0 & -\hat{r} \end{bmatrix}.$$

The solution of (4.18) is a linear combination of terms of the form

$$\mathbf{w}_i e^{\lambda_i \tau}, \quad i = 1, 2, 3, 4$$

where the λ_i are eigenvalues of $\mathbf{A}$, i.e. they are the roots of the characteristic equation

$$\det(\mathbf{A} - \lambda\mathbf{I}) = 0,$$

and $\mathbf{w}_i$ is the eigenvector associated with the eigenvalue λ_i.

$\lambda = -\hat{r}$ is one eigenvalue. To find the other eigenvalues, it is necessary to solve

$$\lambda^3 + (\alpha + \tfrac{a^2}{c^2} + \delta + d + \tfrac{1}{3})\lambda^2 + \left[(\alpha + \tfrac{a^2}{c^2})(\delta + \tfrac{1}{3}) + d(\alpha + \tfrac{a^2}{c^2} + \delta + \tfrac{1}{3})\right]\lambda + d(\alpha + \tfrac{a^2}{c^2})(\delta + \tfrac{1}{3}) - \tfrac{Ka^2}{3c^2} = 0. \quad (4.19)$$

For this steady state to be stable, the roots of the characteristic equation (4.19) must have negative real parts. Denoting

$$\begin{aligned} a_1 &= (\alpha + \frac{a^2}{c^2} + \delta + d + \frac{1}{3}) \\ a_2 &= (\alpha + \frac{a^2}{c^2})(\delta + \frac{1}{3}) + d(\alpha + \frac{a^2}{c^2} + \delta + \frac{1}{3}) \\ a_3 &= d(\alpha + \frac{a^2}{c^2})(\delta + \frac{1}{3}) - \frac{Ka^2}{3c^2} \end{aligned}$$

and applying the Routh-Hurwitz criteria [23], the roots of (4.19) have negative real parts if and only if

(i) all coefficients a_1, a_2 and a_3 are positive,

$$\Rightarrow \quad d(\alpha + \frac{a^2}{c^2})(\delta + \frac{1}{3}) > \frac{Ka^2}{3c^2}$$

since a_1 and a_2 are clearly positive, and

(ii) $a_1 a_2 - a_3 > 0$.

When expression (ii) is expanded and simplified, it is positive for all positive values of parameters α, a, c, δ, d and K. Therefore the condition that this steady state be stable is that condition (i) is satisfied, i.e.

$$d(\alpha + \frac{a^2}{c^2})(\delta + \frac{1}{3}) - \frac{Ka^2}{3c^2} > 0.$$

By choosing suitable values for proportions of death of viable buds, α, incipient branches, δ, and growing points, d, the clover population can be forced to die out. However, for typical values of these parameters the above inequality does not hold, and in general the 'extinct' steady state is locally unstable.

Stability of 'finite' steady state

For simpler notation, write

$$V = x$$

$$I = y$$

$$G = z$$

with steady state values indicated by an asterisk, '*' (i.e. x^*, y^*, z^*).
[Note: for the 'extinct' steady state, $x^* = y^* = z^* = 0$].

Linearising around the 'finite' steady state by putting

$$x = x^* + v$$

$$y = y^* + i$$

$$z = z^* + g$$

$$s = s^* + \sigma$$

and ignoring second and higher-order terms, the linear system obtained is

$$\begin{aligned}
\frac{dv}{d\tau} &= -(\alpha + \frac{a^2}{c^2 + z^{*2}})v + \left(\frac{2a^2x^*z^*}{(c^2 + z^{*2})^2} + K\right)g \\
&\quad + \frac{2a^2x^*z^{*2}}{(c^2 + z^{*2})^2}\sigma \qquad (4.20) \\
\frac{di}{d\tau} &= \frac{a^2}{c^2 + z^{*2}}v - (\delta\gamma y^{*(\gamma-1)} + \frac{1}{3})i - \frac{2ax^*z^*}{(c^2 + z^{*2})^2}g \\
&\quad - \frac{2a^2x^*z^{*2}}{(c^2 + z^{*2})^2}\sigma \qquad (4.21) \\
\frac{dg}{d\tau} &= \frac{1}{3}i - dg \qquad (4.22) \\
\frac{d\sigma}{d\tau} &= -\hat{r}\sigma. \qquad (4.23)
\end{aligned}$$

Using the same process as that used for the 'extinct' steady state, one of the eigenvalues of the system (4.20)–(4.23) is $\lambda = -\hat{r}$. To find the other eigenvalues, the following equation must be solved:

$$\begin{aligned}\lambda^3 &+ (\alpha + \frac{a^2}{c^2 + z^{*2}} + \delta + d + \frac{1}{3})\lambda^2 \\ &+ \left[(\alpha + \frac{a^2}{c^2 + z^{*2}})(\delta + \frac{1}{3} + d) + d(\delta + \frac{1}{3}) + \frac{2a^2x^*z^*}{3(c^2 + z^{*2})^2}\right]\lambda \\ &+ d(\alpha + \frac{a^2}{c^2 + z^{*2}})(\delta + \frac{1}{3}) + \frac{2a^2x^*z^*\alpha}{3(c^2 + z^{*2})^2} - \frac{Ka^2}{3(c^2 + z^{*2})} = 0. \quad (4.24)\end{aligned}$$

From the Routh-Hurwitz criteria, the solutions have negative real parts if, and only if, all coefficients a_1, a_2 and a_3 are positive and $a_1a_2 - a_3 > 0$, where

$$\begin{aligned}a_1 &= (\alpha + \frac{a^2}{c^2 + z^{*2}} + \delta + d + \frac{1}{3}) \\ a_2 &= (\alpha + \frac{a^2}{c^2 + z^{*2}})(\delta + \frac{1}{3} + d) + d(\delta + \frac{1}{3}) + \frac{2a^2x^*z^*}{(c^2 + z^{*2})^2} \\ a_3 &= d(\alpha + \frac{a^2}{c^2 + z^{*2}})(\delta + \frac{1}{3}) + \frac{2\alpha a^2x^*z^*}{3(c^2 + z^{*2})^2} - \frac{Ka^2}{3(c^2 + z^{*2})}.\end{aligned}$$

(i) All coefficients are positive,

$$\Rightarrow \quad d(\alpha + \frac{a^2}{c^2 + z^{*2}})(\delta + \frac{1}{3}) + \frac{2\alpha a^2x^*z^*}{3(c^2 + z^{*2})^2} > \frac{Ka^2}{3(c^2 + z^{*2})}$$

since a_1 and a_2 are clearly positive. This simplifies to

$$\begin{aligned}\frac{2a^2z^{*2}\alpha}{\alpha(c^2 + z^{*2}) + a^2} &> 0 \\ \Rightarrow \quad z^{*2} &> 0\,.\end{aligned}$$

For this to be true, from (4.13) the following inequality must be satisfied:

$$Ka^2 > d(a^2 + \alpha c^2)(3\delta + 1)\,. \quad (4.25)$$

Note: for a physically existing steady state G^*, this inequality is satisfied, otherwise G^* is imaginary.

(ii) $a_1 a_2 - a_3 > 0$.

Using Maple to simplify this expression, it was found to be always positive for positive values of the parameters.

Therefore, when the 'finite' steady state exists, it is locally stable.

4.3.2 With delay

Using the change of variables as given in Section 4.3, the nondimensional form of Equations (4.5)–(4.8) is

$$\frac{dV(\tau)}{d\tau} = K\,G(\tau) - \alpha\,V(\tau) - \frac{a^2\,V(\tau)}{c^2 + [s(\tau)\,G(\tau)]^2} \tag{4.26}$$

$$\frac{dI(\tau)}{d\tau} = \frac{a^2\,V(\tau)}{c^2 + [s(\tau)G(\tau)]^2} - \delta\,[I(\tau)]^\gamma - \frac{a^2\,V(\tau-2)\,e^{-2\delta}}{c^2 + [s(\tau-2)G(\tau-2)]^2} \tag{4.27}$$

$$\frac{dG(\tau)}{d\tau} = \frac{a^2\,V(\tau-2)\,e^{-2\delta}}{c^2 + [s(\tau-2)\,G(\tau-2)]^2} - d\,G(\tau) \tag{4.28}$$

$$\frac{ds(\tau)}{d\tau} = \hat{r}\,s(\tau)\,(1 - s(\tau))\,. \tag{4.29}$$

To find the steady states of (4.26)–(4.29) it is necessary to solve

$$\frac{dV}{d\tau} = \frac{dI}{d\tau} = \frac{dG}{d\tau} = \frac{ds}{d\tau} = 0$$

and assume

$$V(\tau-2) = V(\tau),\ G(\tau-2) = G(\tau),$$

$$s(\tau-2) = s(\tau)$$

as $\tau \to \infty$.

Only considering $s_{ss} = 1$, the steady states are:

(i) the 'extinct' state

$$(V,\ I,\ G,\ s)_{ss} = (0,\ 0,\ 0,\ 1)$$

and

(ii) the 'finite' state

$$\left(\frac{1}{\alpha}(K - d\exp(2\delta))G^*\,,\ \left[\frac{d}{\delta}(\exp(2\delta) - 1)\,G^*\right]^{\frac{1}{\gamma}},\ G^*,\ 1\right)$$

where

$$G^* = \left[\frac{a^2}{d\alpha}(K\exp(-2\delta) - d) - c^2\right]^{\frac{1}{2}}. \tag{4.30}$$

[Note: here, G^* is independent of γ. Compare equation (4.30) with the equation immediately preceding (4.13) which determines G^* in the no-delay case.]

In a similar manner to the stability analysis for the grass model of Chapter 3, linearisation leads to systems of the form

$$\frac{d\mathbf{x}}{d\tau} = \mathbf{A}\mathbf{x}(\tau) + \mathbf{B}\mathbf{x}(\tau - 2)$$

where here

$$\mathbf{x}(\tau) = \begin{bmatrix} v(\tau) \\ i(\tau) \\ g(\tau) \\ \sigma(\tau) \end{bmatrix}$$

and $\mathbf{A}$ and $\mathbf{B}$ are 4×4 matrices, with constant entries.

Assuming solutions are of the form

$$\mathbf{x} = \mathbf{k}e^{\lambda\tau} \qquad \text{where } \mathbf{k} \text{ is a constant vector,}$$

then there are nonzero solutions for $\mathbf{k}$ only if λ satisfies the characteristic equation

$$\det[\mathbf{A} + \mathbf{B}e^{-2\lambda} - \lambda\mathbf{I}] = 0.$$

Stability of 'extinct' state

The following linear system is obtained for determining the stability of the 'extinct' state:

$$\frac{dv(\tau)}{d\tau} = Kg(\tau) - [\alpha + \frac{a^2}{c^2}]\, v(\tau) \tag{4.31}$$

$$\frac{di(\tau)}{d\tau} = \frac{a^2}{c^2} v(\tau) - \delta i(\tau) - \frac{a^2}{c^2} e^{-2\delta}\, v(\tau - 2) \tag{4.32}$$

$$\frac{dg(\tau)}{d\tau} = \frac{a^2}{c^2} e^{-2\delta}\, v(\tau - 2) - dg(\tau) \tag{4.33}$$

$$\frac{d\sigma(\tau)}{d\tau} = -\hat{r}\,\sigma(\tau). \tag{4.34}$$

Equations (4.31)–(4.34) can be written as

$$\frac{d\mathbf{x}}{d\tau} = \begin{bmatrix} -(\alpha + \frac{a^2}{c^2}) & 0 & K & 0 \\ \frac{a^2}{c^2} & -\delta & 0 & 0 \\ 0 & 0 & -d & 0 \\ 0 & 0 & 0 & -\hat{r} \end{bmatrix} \mathbf{x}(\tau) + \begin{bmatrix} 0 & 0 & 0 & 0 \\ -\frac{a^2}{c^2} e^{-2\delta} & 0 & 0 & 0 \\ \frac{a^2}{c^2} e^{-2\delta} & 0 & 0 & 0 \\ 0 & 0 & 0 & 0 \end{bmatrix} \mathbf{x}(\tau - 2)$$

where

$$\mathbf{x}(\tau) = \begin{bmatrix} v(\tau) \\ i(\tau) \\ g(\tau) \\ \sigma(\tau) \end{bmatrix}.$$

The characteristic equation is

$$\det \begin{bmatrix} -(\alpha + \frac{a^2}{c^2}) & 0 & K & 0 \\ \frac{a^2}{c^2}(1 - e^{-2(\delta+\lambda)}) & -\delta & 0 & 0 \\ \frac{a^2}{c^2} e^{-2(\delta+\lambda)} & 0 & -d & 0 \\ 0 & 0 & 0 & -\hat{r} \end{bmatrix} = 0$$

which simplifies to

$$(-\delta - \lambda)(-\hat{r} - \lambda)\left((\alpha + \frac{a^2}{c^2} + \lambda)(d + \lambda) - \frac{Ka^2}{c^2} e^{-2(\delta+\lambda)}\right) = 0.$$

The eigenvalues are $\lambda = -\delta,\ -\hat{r}$ and the solutions of

$$\lambda^2 + (\alpha + \frac{a^2}{c^2} + d)\lambda + d(\alpha + \frac{a^2}{c^2}) = \frac{Ka^2}{c^2}e^{-2(\delta+\lambda)}. \tag{4.35}$$

It is now shown that there is a real solution to this equation. The right hand side of (4.35) is an exponentially decaying positive function which is decreasing for all λ. The left hand side of (4.35) is a quadratic which is increasing for all $\lambda > -\frac{1}{2}(\alpha + a^2/c^2 + d)$. Let

$$f(\lambda) = \lambda^2 + (\alpha + \frac{a^2}{c^2} + d)\lambda + d(\alpha + \frac{a^2}{c^2})$$

and

$$g(\lambda) = \frac{Ka^2}{c^2}e^{-2(\delta+\lambda)}.$$

Figure 4.5 shows the cases where

(a) $g(0) > f(0)$

(b) $g(0) < f(0)$.

The intersection of these two functions is at a negative λ value when $g(0) < f(0)$ (curve (b) in Figure 4.5), i.e. when

$$d(\alpha + \frac{a^2}{c^2}) > K\frac{a^2}{c^2}e^{-2\delta}.$$

If this inequality is not satisfied then the real solution of (4.35) is positive (curve (a) in Figure 4.5).

Conjecture 1 *There are an infinite number of complex solutions to (4.35), and the real parts of these solutions are always less than the solution found from Figure 4.5.*

If this conjecture holds then whenever

$$d(\alpha + \frac{a^2}{c^2}) > K\frac{a^2}{c^2}e^{-2\delta}$$

the 'extinct' steady state is locally stable.

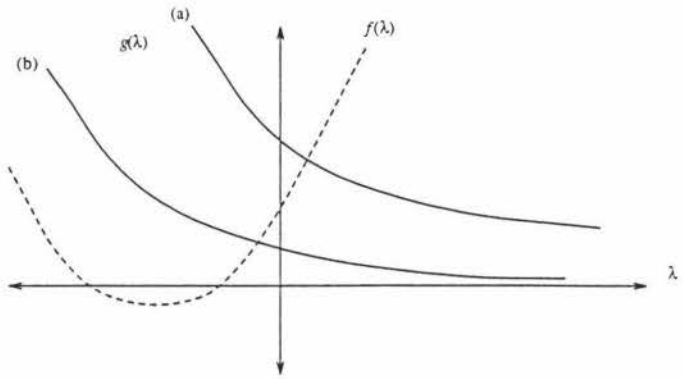

Figure 4.5: λ real for 'extinct' steady state

Stability of 'finite' state

By considering a small perturbation and using the same notation as before the following linear system is obtained:

$$\begin{aligned}
\frac{dv(\tau)}{d\tau} &= -(\alpha + \frac{a^2}{c^2 + z^{*2}})v(\tau) + \left(\frac{2a^2x^*z^*}{[c^2 + z^{*2}]^2} + K\right) g(\tau) \\
&\quad + \frac{2a^2x^*z^{*2}}{[c^2 + z^{*2}]^2}\sigma(\tau) \qquad (4.36) \\
\frac{di(\tau)}{d\tau} &= \frac{a^2}{c^2 + z^{*2}}[v(\tau) - e^{-2\delta}v(\tau - 2)] - \delta i(\tau) \\
&\quad - \frac{2a^2x^*z^*}{[c^2 + z^{*2}]^2}[g(\tau) - e^{-2\delta}g(\tau - 2)] \\
&\quad - \frac{2a^2x^*z^{*2}}{[c^2 + z^{*2}]^2}[\sigma(\tau) - e^{-2\delta}\sigma(\tau - 2)] \qquad (4.37) \\
\frac{dg(\tau)}{d\tau} &= \frac{a^2e^{-2\delta}}{c^2 + z^{*2}}v(\tau - 2) - \frac{2a^2x^*z^*}{[c^2 + z^{*2}]^2}e^{-2\delta}g(\tau - 2) - dg(\tau) \\
&\quad - \frac{2a^2x^*z^*}{[c^2 + z^{*2}]^2}e^{-2\delta}\sigma(\tau - 2) \qquad (4.38) \\
\frac{d\sigma(\tau)}{d\tau} &= -\hat{r}\sigma(\tau). \qquad (4.39)
\end{aligned}$$

This linear system can be written in the form

$$\frac{d\mathbf{x}}{d\tau} = \mathbf{A}\mathbf{x}(\tau) + \mathbf{B}\mathbf{x}(\tau - 2)$$

where

$$\mathbf{A} = \begin{bmatrix} -\left(\alpha + \frac{a^2}{c^2+z^{*2}}\right) & 0 & \left(\frac{2a^2x^*z^*}{[c^2+z^{*2}]^2} + K\right) & \frac{2a^2x^*z^*}{[c^2+z^{*2}]^2} \\ \frac{a^2}{c^2+x^{*2}} & -\delta & \frac{-2a^2x^*z^*}{[c^2+z^{*2}]^2} & \frac{-2a^2x^*z^*}{[c^2+z^{*2}]^2} \\ 0 & 0 & -d & 0 \\ 0 & 0 & 0 & -\hat{r} \end{bmatrix},$$

$$\mathbf{B} = \begin{bmatrix} 0 & 0 & 0 & 0 \\ \frac{-a^2e^{-2\delta}}{c^2+x^{*2}} & 0 & \frac{2a^2x^*z^*e^{-2\delta}}{[c^2+z^{*2}]^2} & \frac{2a^2x^*z^*e^{-2\delta}}{[c^2+z^{*2}]^2} \\ \frac{a^2e^{-2\delta}}{c^2+x^{*2}} & 0 & \frac{-2a^2x^*z^*e^{-2\delta}}{[c^2+z^{*2}]^2} & \frac{-2a^2x^*z^*e^{-2\delta}}{[c^2+z^{*2}]^2} \\ 0 & 0 & 0 & 0 \end{bmatrix}$$

and

$$\mathbf{x}(\tau) = \begin{bmatrix} v(\tau) \\ i(\tau) \\ g(\tau) \\ \sigma(\tau) \end{bmatrix}.$$

From the characteristic equation

$$\det(\mathbf{A} + \mathbf{B}e^{-2\lambda} - \lambda\mathbf{I}) = 0$$

two eigenvalues are $\lambda_1 = -\delta$ and $\lambda_2 = -\hat{r}$. To find the other eigenvalues, it is necessary to solve

$$\lambda^2 + (\alpha + \frac{a^2}{c^2+z^{*2}} + d)\lambda + d(\alpha + \frac{a^2}{c^2+z^{*2}}) =$$

$$\frac{Ka^2e^{-2(\delta+\lambda)}}{c^2+z^{*2}} - \frac{2a^2x^*z^*e^{-2(\delta+\lambda)}}{[c^2+z^{*2}]^2}(\alpha+\lambda). \qquad (4.40)$$

For this steady state to be locally stable, the real part of the solutions to (4.40) must be negative. To examine the nature of these solutions, eliminate x^* and z^* by substituting

$$x^* = \frac{1}{\alpha}(K - d\,e^{2\delta})\,z^*$$

and

$$z^* = \left[\frac{a^2}{d\alpha}(K\exp(-2\delta) - d) - c^2\right]^{\frac{1}{2}} \quad \text{(See Equation 4.30)}$$

into Equation 4.40.

Let

$$\begin{aligned} f(\lambda) &= \lambda^2 + \left(\alpha + \frac{d\alpha}{Ke^{-2\delta} - d} + d\right)\lambda + d\left(\alpha + \frac{d\alpha}{Ke^{-2\delta} - d}\right), \\ g(\lambda) &= \left[\frac{Kd\alpha e^{-2\delta}}{Ke^{-2\delta} - d} - 2d\left(1 - \frac{\alpha dc^2}{(Ke^{-2\delta} - d)a^2}\right)(\alpha + \lambda)\right] e^{-2\lambda} \\ &= [M - N(\alpha + \lambda)]e^{-2\lambda} \end{aligned}$$

where

$$\begin{aligned} M &= \frac{Kd\alpha e^{-2\delta}}{Ke^{-2\delta} - d} \\ N &= 2d\left(1 - \frac{\alpha dc^2}{(Ke^{-2\delta} - d)a^2}\right). \end{aligned}$$

For existence of this steady state,

$$\begin{aligned} & K\frac{a^2}{c^2}e^{-2\delta} > d(\alpha + \frac{a^2}{c^2}) \\ \Rightarrow \quad & 1 - \frac{\alpha dc^2}{(Ke^{-2\delta} - d)a^2} > 0 \\ \Rightarrow \quad & 2d\left(1 - \frac{\alpha dc^2}{(Ke^{-2\delta} - d)a^2}\right) > 0, \end{aligned}$$

i.e. N is always positive.

This means that, as $\lambda \to -\infty$, $g(\lambda) \to +\infty$ and also $g(\lambda) \to 0^-$ as $\lambda \to +\infty$. The graph of $g(\lambda)$ intersects the λ-axis once only at

$$\begin{aligned} \lambda_0 &= \frac{K\alpha e^{-2\delta}a^2}{2[(Ke^{-2\delta} - d)a^2 - \alpha dc^2]} - \alpha \\ &= \frac{M}{N} - \alpha. \end{aligned}$$

It is easy to show that $g(\lambda)$ has only one local minima at $\lambda = \lambda_0 + \frac{1}{2}$. The above information is summarised in Figure 4.6. This figure shows $g(\lambda)$ for

(a) $g(0) > f(0)$

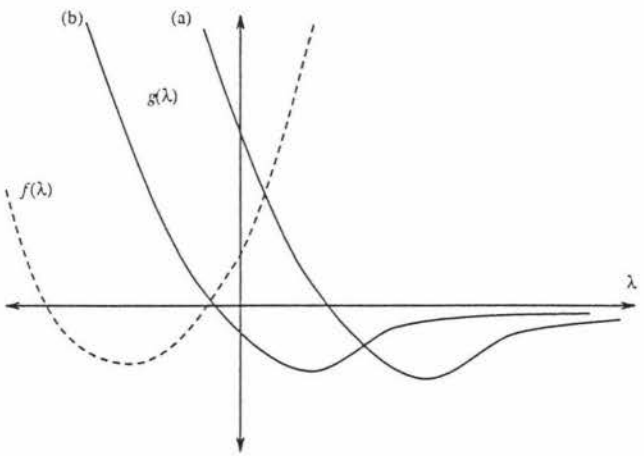

Figure 4.6: λ real for 'finite' steady state

(b) $g(0) < f(0)$.

Now $f(\lambda)$ and $g(\lambda)$ intersect at a negative λ when $f(0) > g(0)$, i.e.

$$d(\alpha + \frac{d\alpha}{Ke^{-2\delta} - d}) > \frac{Kd\alpha e^{-2\delta}}{Ke^{-2\delta} - d} - 2d\left[1 - \frac{\alpha dc^2}{(Ke^{-2\delta} - d)a^2}\right]\alpha.$$

This simplifies to give

$$K\frac{a^2}{c^2}e^{-2\delta} > d(\alpha + \frac{a^2}{c^2}).$$

From Equation (4.30), this is the inequality required for G^* to exist.

Conjecture 2 *There are an infinite number of complex solutions to (4.40) with real parts always less than the real solution found above.*

If this conjecture holds then whenever

$$K\frac{a^2}{c^2}e^{-2\delta} > d(\alpha + \frac{a^2}{c^2})$$

the 'finite' steady state is locally stable.

Therefore, as for the grass model in the preceding chapter, the 'finite' steady state is locally stable whenever it exists.

4.4 Global Stability

To study the global behaviour of the systems (4.1)–(4.4) and (4.5)–(4.8), the only effective method is to compute solutions via the numerical method described in Section 4.2 for various initial population sizes VB, IB, GP and growing point size, S. Figure 4.7 (model without delay) shows the convergence of trajectories towards the 'finite' steady state from six different initial population sizes.

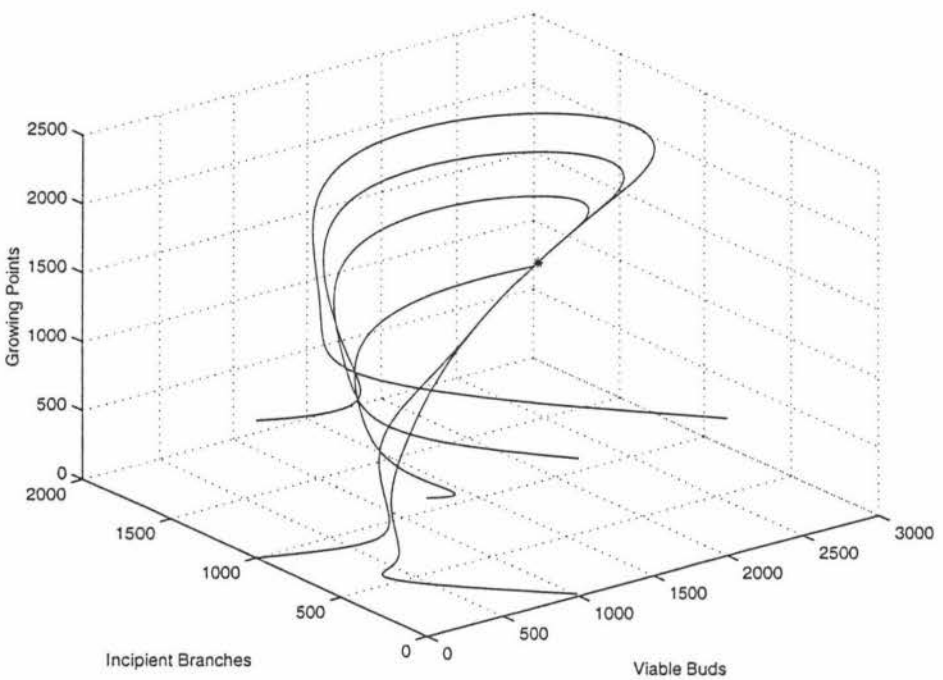

* steady state point

Figure 4.7: Trajectories *(Without delay)*

Figure 4.8 shows similar results obtained from the model with delay. Again, the trajectories converge to the 'finite' steady state. However, it is interesting to note that if initially there are no viable buds, VB, and no growing points, GP, the 'extinct' steady state is obtained, i.e. the incipient branch population dies out. Looking at (4.5)–(4.8) it is evident that the populations cannot grow without viable buds and growing points. The only outcome in this case is an

(exponentially) decreasing incipient branch population, with the viable bud and growing point populations remaining at zero.

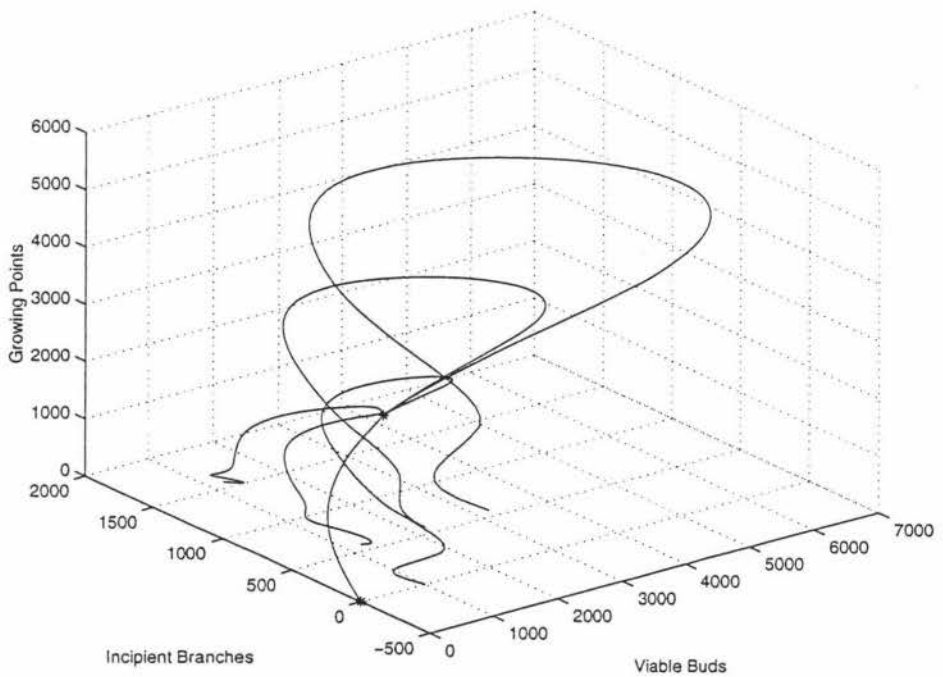

* steady state points

Figure 4.8: Trajectories *(With delay)*

4.5 Harvesting

Harvesting was simulated by periodically reducing the size of growing points to their original size. Figures 4.9 and 4.10 show the numerical solutions of the model without delay and with delay, respectively, where the original size $S_0 = 0.02$ g, and the harvesting interval is 30 days. The densities of viable buds, incipient branches and growing points are higher than the densities obtained from the simulations without harvesting (Figure 4.3).

The results from simulating harvesting are similar. For example, the only significant difference between Figures 4.9 (no delay) and 4.10 (delay) is a small decrease

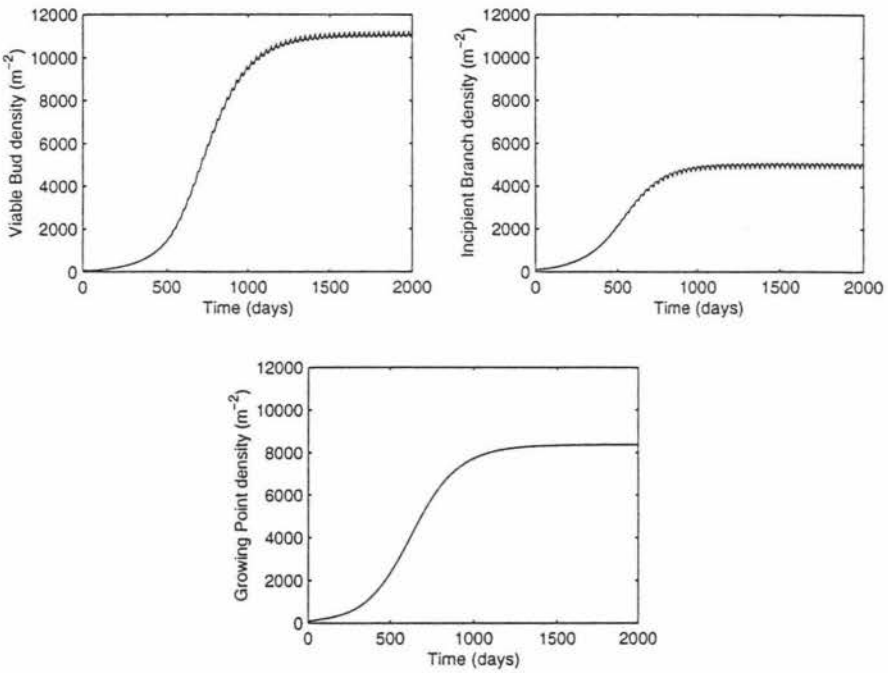

Figure 4.9: Harvesting *(Without delay)*

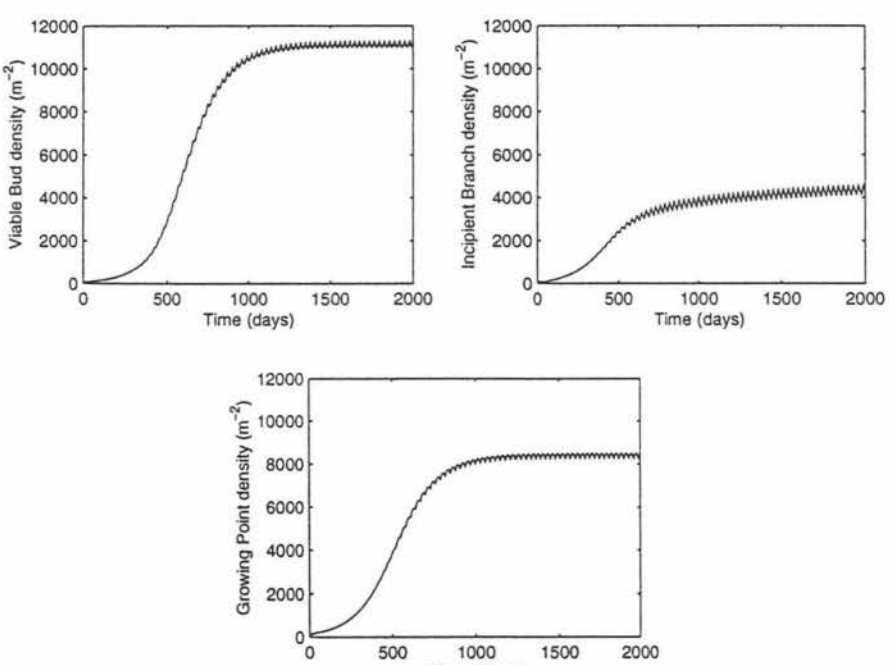

Figure 4.10: Harvesting *(With delay)*

in incipient branch density after 2000 days. The oscillations in numbers between harvests do however appear slightly larger in the delay model, especially in the plot for growing points of Figure 4.10.

4.6 Summary and Comments

This chapter investigated two models constructed to describe the growth of white clover based on growing point numbers. Although the delay model would appear to be the more biologically realistic of the two, all analytic and numerical results reveal little qualitative difference between them.

A steady state analysis revealed two steady states, a stable 'finite' state and unstable 'extinct' state. A threshold condition was found for each of the models determining which of the steady states was eventually reached.

Simulating harvesting resulted in an increase in viable buds, incipient branches and growing points.

This clover model exhibits in general terms the behaviour of clover plants in the field (Newton, personal communication). These include

1. steady state population size

2. harvesting increases growing point number.

Chapter 5

Summary

5.1 Conclusions

The principal aim of this thesis was to construct a model which can be used to address the problem of ryegrass non-persistence and lower than desirable proportions of white clover in pastures. Due to the difficulty of this problem, it has been divided into two smaller problems of modelling the behaviour of grass and clover as separate populations.

Chapter 2 outlined an example of a physiological approach in modelling ryegrass growth. One of the drawbacks of many physiological models is the large number of state variables and parameters. Estimation of these parameters can be difficult. Although there are numerous software packages available, with which numerical simulations can be calculated, mathematical analysis is difficult.

Chapters 3 and 4 take a population dynamics approach to the problem. Although the behaviour of grass and clover are modelled separately the models are constructed along similar lines. The parent tillers of ryegrass are thought to be analogous to the growing points of clover. Daughter tillers are analogous to incipient branches. However, the ryegrass model does not have a term comparable to viable buds. It is hoped that the similarity in the form of these two dynamical

systems will facilitate the merging of the two models. It is only after the construction of a single model that the questions of co-existence and persistence can be addressed.

From a mathematical viewpoint these models are not difficult to analyse. Both models have two steady states when a certain threshold condition is satisfied: a zero, or extinct, steady state and a finite steady state. The finite steady state is locally stable whenever it exists. However, when harvesting is included, it appears from the simulations that cyclic long-term behaviour is established although this has not been rigorously proven in this thesis.

5.2 Further Work

Grass Model

In the simulations produced in Chapter 3 the leaf appearance rate remained fixed for any single run of the model. In practice, leaf appearance rates are strongly related to temperature and therefore vary throughout the year. This could be incorporated into the model by making leaf appearance rate a periodic function of time.

Reproductive development is an important feature of grass growth. This could be incorporated into the model by introducing a reproductive tiller pool and a size pool for these reproductive tillers. Because reproductive development takes place only in the spring, this pool operates only during this time.

Clover

The bud appearance rate of Chapter 4 remains fixed throughout each simulation in the clover model. In practice, this varies seasonally and can be incorporated into

the model in a fashion similar to the leaf appearance rate of the ryegrass model.

Combining Models

The ultimate aim is to combine the grass and clover models so as to predict the balance of species, persistence and productivity in this mixed species association. This as yet has not been worked out in detail but a possible way to proceed is for the density-dependent birth processes in the two separate models to be dependent on the total mass density of grass and clover. An experiment is under way at AgResearch to test this idea.

Bibliography

[1] Baars, J.A. (1982). Variation in grassland production in the North Island with particular reference to Taranaki. *Proceedings of the New Zealand Grassland Association, 43*, 32–43.

[2] Begon, M., Harper, J.L. and Townsend, C.R. (1990). *Ecology: individuals, populations and communities.* Blackwell Scientific Publications, Oxford.

[3] Begon, M. and Mortimer, M. (1986). *Population ecology: a unified study of animals and plants.* Blackwell Scientific Publications, Oxford.

[4] Bircham, J.S. and Hodgson, J. (1983). The influence of sward conditions on rates of herbage growth and senescence in mixed swards under continuous stocking management. *Grass and Forage Science, 38*, 323–331.

[5] Brereton, A.J. (1992). A description and parameterisation of a dynamic model of tiller appearance and death in perennial ryegrass (Lolium perenne). In *Grasslands and Society*, Ed. L 'tMannetje and J. Frame, pp 247–251. *Proceedings 15th General Meeting of the European Grassland Society,* Wageningen Pers, Wageningen.

[6] Bullock, J.M. (1996). Plant Competition and Population Dynamics. In *The Ecology and Management of Grazing Systems,* Ed J. Hodgson and A.W. Illius, pp. 69–100. CAB International, Wallingford.

[7] Cappuccino, N. (1985). Novel Approaches to the Study of Population Dynamics. In *Population dynamics: new approaches and synthesis,* Ed. N. Cappuccino and P.W. Price, Academic Press, San Diego.

[8] Dayan, E., Van Keulen, H. and Dovrat, A. (1981). Tiller dynamics and growth of rhodes grass after defoliation: A model named TILDYN. *Agro-Ecosystems, 7*, 101–112.

[9] Edelstein-Keshet, (1987). *Mathematical models in biology.* McGraw Hill, New York.

[10] Frame, J. and Newbold, P. (1984). Herbage production from grass/white clover swards. In *Forage Legumes*, Ed. D.J. Thompson, pp. 15–35. Hurley, UK: British Grassland Society Occasional Symposium 16.

[11] Guckenheimer, J., Oster, G.F. and Ipaktchi, A. (1976). The dynamics of density dependent population models. *Journal of Mathematical Biology, 4*, 101–147.

[12] Humphreys, L.R. (1997). *The evolving science of grassland improvement*, Cambridge University Press, Cambridge.

[13] Johnson, I.R., Ameziane, T.E. and Thornley, J.H.M. (1982). A model of grass growth. *Annals of Botany, 51*, 599–609.

[14] Johnson, I.R. and Thornley, J.H.M. (1983). Vegetative crop growth model incorporating leaf area expansion and senescence, and applied to grass. *Plant, Cell and Environment, 6*, 721–729.

[15] Johnson, I.R. and Thornley, J.H.M. (1985). Dynamic model of the response of a vegetative grass crop to light, temperature and nitrogen. *Plant, Cell and Environment, 8*, 485–499.

[16] Jones, M.B., Collett, B. and Brown, S. (1982). Sward growth under cutting and continuous stocking management: sward structure, tiller density and leaf turnover. *Grass and Forage Science, 37*, 67–73.

[17] Laidlaw, A.S. and Reed, K.F.M. (1993). Plant improvement: the evaluation and extension processes. In *Proceedings XVII International Grassland Congress, 1*, 385–392.

[18] Langer, R.H.M. (1979). How Grasses Grow, Institute of Biology, *Studies in Biology, 34*, Edward Arnold.

[19] Louie, K., Clark, H. and Newton, P.C.D. (1997). Using differential equations in biological modelling - a case study for clover. Submitted to *NZ Journal of Agricultural Research.*

[20] McCall, D. G. (1984). A systems approach to research planning for North Island hill country. PhD Thesis, Massey University.

[21] McDonald, N. And Watkinson, A.R. (1981). Models of an annual plant population with a seed bank. *Journal of Theoretical Biology, 93*, 643–653.

[22] Murray, J.D. (1977). Lectures on Nonlinear Differential Equation Models in Biology, (Chap. 4), Clarendon Press, Oxford.

[23] Murray, J.D. (1993). In *Mathematical Biology*, (second, corrected edition). Section A2.1, pp 702–704. Biomathematics Text, Springer-Verlag.

[24] Newton, P.C.D., Hay, M.J.M., Thomas, V.J. and Dick, H.B. (1992). Viability of axillary buds of white clover (Trifolium repens) in grazed pasture. *Journal of Agricultural Science, Cambridge, 119*, 345–354.

[25] Olsen, B.E., Senft, R.L. and Richards, J.H. (1989). A test of grazing compensation and optimisation of crested wheatgrass using a simulation model. *Journal of Range Management, 42(6)*, 458–467.

[26] Pacala, S.W. (1986). Neighbourhood models of plant population dynamics 4. Single species and multi species models of annuals with dormant seeds. *American Naturalist, 128*, 859–878.

[27] Robson, M.J., Parsons, A.J. and Williams, T.E. (1989). Herbage Production. In *Grass - its Production and Utilisation*, Ed. W. Holmes. pp. 7–73. Blackwell Scientific Publications, Oxford.

[28] Silliman, R.P. and Gutsell, J.S. (1958). Experimental exploitation of fish populations, *Fishery Bulletin, Fish Wildlife Service. U. S., 58*, 215–241.

[29] The MathWorks Inc. (1992). *MATLAB Reference Guide. For UNIX Workstations.*

[30] Thornley, J.H.M. (1976). *Mathematical Models in Plant Physiology*, pp 93–95. Academic Press, London, New York.

[31] Watkinson, A.R. (1980). Density dependence in single-species populations of plants. *Journal of Theoretical Biology, 83*, 345–357.

[32] Woodward, S.J.R. (1996). Dynamical systems models and their application to optimising grazing management. In *Agricultural Systems Modelling and Simulation*, Ed. R.M. Peart and R.B. Curry, pp. 1–40. Marcel-Dekker.

[33] Woodward, S.J.R. and Wake, G.C. (1994). A differential-delay model of pasture accumulation and loss in controlled grazing systems. *Mathematical Biosciences, 121*, 37–60.